Rectangular Stress-block Parameters for Fly-ash and Slag Based Geopolymer Concrete

Tung T. Tran, Thong M. Pham, Hong Hao

PII: S2352-0124(19)30006-2
DOI: https://doi.org/10.1016/j.istruc.2019.01.006
Reference: ISTRUC 384

To appear in: *Structures*

Received date: 5 November 2018
Revised date: 24 December 2018
Accepted date: 7 January 2019

Please cite this article as: Tung T. Tran, Thong M. Pham, Hong Hao , Rectangular Stress-block Parameters for Fly-ash and Slag Based Geopolymer Concrete. Istruc (2018), https://doi.org/10.1016/j.istruc.2019.01.006

Rectangular Stress-block Parameters for Fly-ash and Slag Based Geopolymer Concrete

Tung T. Tran[1], Thong M. Pham[2], and Hong Hao[3]

ABSTRACT

Although there has been a numerous quantity of studies investigating the mechanical properties of geopolymer concrete (GPC), parameters for designing GPC structures are still not systematically investigated and carefully justified. ACI rectangular stress-block parameters is able to predict well the strength of conventional concrete structures but their applicability for GPC is questionable. This study aims to establish new sets of rectangular stress-block parameters for GPC with a broad range of the compressive strength up to 66 MPa. The proposed rectangular stress-block parameters in this study are based on two analytical concrete stress-strain models and measured curves from previous studies of GPC materials. The results from this study show that the use of ACI recommendations for concrete structure in designing GPC beams is still acceptable with high accuracy. However, the axial load-carrying capacity of GPC columns computed by ACI parameters deviate significantly from the experimental results while the proposed parameters provide a good correlation with these experimental data. The significant difference is mainly due to the modification of k_3, which is the ratio of concrete strength in real structures to standard cylinder samples. This study suggests that the assumption of k_3=0.9 in previous studies for conventional Portland concrete is not suitable for use in deriving the stress-block parameters of GPC. In some cases, this ratio should be reduced to 0.7 depending on the curing condition.

Key words: Geopolymer concrete; stress block parameters; Beams; Columns.

[1]PhD Scholar, Center for Infrastructural Monitoring and Protection, School of Civil and Mechanical Engineering, Curtin University, Kent Street, Bentley, WA 6102, Australia. Email: thanhtung.tran@postgrad.curtin.edu.au

[2]Research Fellow, Center for Infrastructural Monitoring and Protection, School of Civil and Mechanical Engineering, Curtin University, Kent Street, Bentley, WA 6102, Australia (corresponding author). Email: thong.pham@curtin.edu.au

[3]John Curtin Distinguished Professor, Center for Infrastructural Monitoring and Protection, School of Civil and Mechanical Engineering, Curtin University, Kent Street, Bentley, WA 6102, Australia (corresponding author). Email: hong.hao@curtin.edu.au

1. INTRODUCTION

The process of synthesizing Portland cement which is emitting a large amount of carbon dioxide (CO2) into the atmosphere [1] is one of the main factors contributing to the global warming. In this context, it is necessary to find a new material to replace the conventional but non-environmentally-friendly Portland cement. Currently, geopolymer concrete (GPC), which is produced from industrial by-products such as fly-ash and slags [2], is regarded as a promising solution.

Until now most studies have focused on investigating the mixture design and mechanical properties of GPC [3]. It is demonstrated that GPC has some superior characteristics such as low creep, little drying shrinkage, excellent sulphate and acid sulfuric resistance [4], and better bonding as well as flexural strength [5, 6]. Furthermore, by adjusting the ratio of sodium silicate and sodium hydroxide solution when mixing GPC, the bond strength between GPC and steel reinforcement could increase up to 36% [7]. In contrast, some available studies also specified the disadvantages in mechanical characteristics of GPC. The experimental findings of these studies reported the lower elastic modulus of GPC compared to those of ordinary Portland concrete (OPC) with the same compressive strength [8-10]. Therefore, the equations for estimating the elastic modulus of OPC in current standards have a tendency of overestimating the actual elastic modulus of GPC [8]. In addition, a more brittle response in mechanical behaviour of GPC than OPC was observed in the experimental tests [11-13]. Most studies investigating the compressive stress-strain behaviour of GPC also reported significant differences between GPC and OPC [10, 14, 15]. Due to such distinction of the material behaviour between GPC and OPC, it is essential to examine the suitability of applying the current design methods of OPC for GPC.

In contrast to the number of previous studies on the mechanical properties of GPC, investigations of the behaviours of structures made of GPC are still limited and contrary

findings were reported. The behaviour of GPC beams were investigated in several experimental studies [16-22] while other studies examined the structural performance of GPC columns [23-26]. In general, these studies showed the structural response of the GPC beams and columns was almost identical to that of OPC and thus concluded that the current design codes and models for OPC structures can be applied to calculate the strength of GPC beams and columns. Nevertheless, a recent investigation on the behaviour of ambient cured GPC columns subjected to axial load and uniaxial bending demonstrated that the sectional analysis procedure based on AS3600 standards considerably overestimated the strength of these columns compared to test results [27]. This variation indicates that the design procedures in available standards for OPC structures are inaccurate in estimating the capacity of GPC structures.

To estimate the load-carrying capacity of reinforced OPC beams and columns, the ACI 318-11 building code [28] recommended rectangular stress-block parameters that can be derived from the tests of eccentrically loaded columns [29] or from an analytic stress-strain curve [30]. From the obvious difference of compressive stress-strain relationship between GPC and OPC, it is evident that the stress-block parameters of GPC cannot be the same as OPC. Hence this paper aims to formulate the equations of rectangular stress-block parameters for GPC. The proposed equations are used to estimate bending moment capacity of beams and the axial load-moment interaction diagrams of columns. The analytical estimations are verified against the test results from the previous studies in the literature [16, 23, 27].

2. RESEARCH SIGNIFICANCE

There has been a limited number of studies evaluating and proposing the equivalent stress-block parameters for fly-ash based GPC until now [31, 32]. In the first study, the Popovics's stress-strain curve for modelling stress-strain relationship of fly-ash based GPC was calibrated by Prachasaree et al. [31] to derive a set of equivalent stress-block parameters.

Meanwhile, a combined axial-flexural test proposed by Hognestad et al. [29] was conducted in the second study to determine experimentally the equivalent stress-block parameters of GPC. Although the results calculated by those parameters demonstrated a good prediction of moment capacity of GPC beams, there has been no verification of reliability of these parameters in calculating the strength of GPC columns. Moreover, a drastic difference in stress-strain behaviour of GPC made of ground granulated blast furnace slag (GGBFS) and fly-ash with OPC was reported in the previous study [10] and illustrated in Fig. 1. The performance of GPC after the peak stress is extremely brittle compared to OPC. The same phenomenon has been observed in previous experiments, and has been attributed to the high prevalence of micro-cracking in GPC made of GGBFS [13]. Owning to such differences, it is apparent that the use of stress-block parameters in current design codes for OPC likely leads to unsafe predictions for GPC as reported in an aforementioned study [27]. With this motivation, a set of rectangular stress-block parameters for GPC column and beam is proposed in this study. In literature, the rectangular stress-block parameters were derived from an analytical stress-strain model [30, 33]. Therefore, this study adopts the two modified-Popovics stress-strain curves for GPC in the previous studies [10, 24] to establish two sets of rectangular stress-block parameters. Furthermore, based on measured curves from the published experimental results [8, 10, 13, 34] which were summarized in Table 1, the third set of rectangular stress-block parameters is also derived. Then, the three sets of rectangular stress-block parameters are compared and the most suitable set for GPC design is determined.

Fig. 1. Comparison of stress-strain curves of cylinder tests of GPC and OPC

Table 1-Summary of experimental data of compressive cylinder tests

3. REVIEW OF STRESS-BLOCK PARAMETERS

The assumptions for simplification of designing the concrete members subjected to bending moment are described in Fig. 2. The strain distribution (Fig. 2b) on the whole section is linear and the tensile stress of concrete is neglected. Concrete stress in the compressive zone is distributed according to the measured stress-strain curve that can be expressed mathematically by three parameters, i.e., k_1, k_2 and k_3 (Fig. 2c) or is assumed having a rectangular shape in which the stress-block parameters are defined by two parameters α and β (Fig. 2d). To determine these parameters, a comprehensive test program of eccentrically loaded C-shaped columns was conducted by Hognestad et al. [29] and the results had been adopted by the ACI 318 building code and recommended for concrete structure design until today. Currently, ACI 318-11 standard [28] recommends 0.85 for the parameter α while β has the value of 0.85 when the concrete compressive strength is less than 28 MPa and decreases by 0.05 for each 7 MPa but is limited by 0.65.

Although the research by Hognestad et al. [29] was comprehensive and provided a relatively accurate design calculations, it had just considered the concrete with normal strength under 60 MPa. In terms of high strength concrete, Ibrahim and MacGregor conducted 20 tests of eccentrically loaded columns to obtain parameters k_1, k_2 and k_3 and then derived the equivalent rectangular stress-block parameters α and β [35, 36]. Their research indicated the ACI value of 0.85 for parameter α was too high and not conservative to calculate the column capacity of high strength concrete. This can be explained by the fact that the actual stress-strain relationship of high strength concrete approaches to a triangular shape when the compressive strength increases. As a result, the value of α reduced considerably until reaching 0.725. In addition, the lower bound value of β derived from ACI equation is too small for high strength concrete. Hence, the internal level arm becomes too big and the

moment capacity is overestimated. Based on experimental data and findings from regression analysis, they suggested that the parameters α and β could be expressed as follows:

$$\alpha = 0.85 - \frac{f_c^{'}}{800} \geq 0.725 \quad (1)$$

$$\beta = 0.95 - \frac{f_C^{'}}{400} \geq 0.7 \quad (2)$$

where $f_c^{'}$ (MPa) is the compressive strength of concrete.

Fig. 2. Assumptions for concrete structure designs

Moreover, the premature cover spalling in high strength concrete columns was recorded in the previous studies [35, 37]. Such a phenomenon leads to a strength loss in the columns. To ensure the safety in design, some researchers proposed new sets of stress-block parameters incorporating the early cover spalling of high strength concrete for calculating the column capacity. Ozbakkaloglu and Saatcioglu [38] introduced the effect of cover spalling through multiplying k_3 by a parameter k_4 to predict the strength of high strength concrete column under axial load.

$$k_4 = \gamma + (1-\gamma)\frac{A_c}{A_g} \leq 0.95 \quad (3)$$

$$\gamma = 1.1 - 0.007 f_c^{'} \leq 0.8 \quad (4)$$

where A_c is the area of core concrete and A_g is the gross area of concrete section. Nevertheless, in the case of eccentrically loaded columns, they assumed that the cover spalling of the columns under bending is not likely to happen and thus the parameter k_4 in Eq. (3) becomes 1. In contrast, the results in the previous study by Bae and Bayrak [39] demonstrated a capacity reduction of high strength concrete columns under eccentric loads

due to the early cover spalling and then proposed a new set of equivalent rectangular stress-block parameters considering this phenomenon [40]. Their stress-block parameters are relatively accurate to calculate the axial load-carrying capacity of high strength concrete columns.

A previous study also indicated transverse reinforcement ratio influences the capacity of high strength concrete column [41]. From the tests in that study, it is noted that the flexural strength of columns confined with the reasonable transverse reinforcement ratio exceeded the calculated capacity based on rectangular stress-block parameters derived by Ibrahim and MacGregor [36]. By that reason, a set of rectangular stress-block parameters for unconfined and confined concrete has been proposed by Karthik and Mander [30]. In order to obtain the rectangular stress-block model, they suggested a new and simplified analytical stress-strain curve for a wide range of concrete strengths and confining stresses. Recently, a rectangular stress-block model was proposed to calculate the flexural strength of steel fibre reinforced concrete beams [42]. By using that model, the calculated moment capacity of beams was fairly accurate compared to the experimental findings.

In spite of a large amount of studies on the rectangular stress-block parameters for conventional Portland concrete with a wide range of compressive strength, only a few studies on stress-block parameters for fly-ash based GPC under heated curing condition has been reported in the literature [31, 32]. Those studies proposed new sets of parameters defining the equivalent rectangular stress-block. Their results gave a better prediction for flexural capacity of GPC beams. However, they suggested that it is reasonable to use the parameters from ACI 318-11 building code [28] since it still provided a conservative estimation. In contrast, it seems that the strength of GPC columns calculated by the stress-block parameters from ACI 318-11 code [28] is not conservative. An aforementioned study [27] indicated a significant overestimation of the load-carrying capacity of GPC columns when using the current design

codes. In addition, in their experiments, the early cover spalling of columns was observed in most cases even though the normal-strength concrete of about 35 MPa was used. It is worth mentioning that this phenomenon has been only recorded in high strength Portland concrete columns. Owing to such a distinction in structural performance, it is evident that the rectangular stress-block parameters in the current design codes for Portland concrete are not necessarily suitable for designing GPC structures. With this observation, this research intends to develop a new and rational set of equivalent rectangular stress-block parameters for GPC structures. The equations of these parameters are established based on integrating the analytical stress-strain curves obtained from previous studies with GPC [10, 24] or measured curves from the published experimental results [8, 10, 13, 34].

4. ANALYTICAL STRESS-STRAIN CURVES FOR GEOPOLYMER CONCRETE

Based on a review on stress-strain models of GPC, the following two constitutive models are adopted to derive rectangular stress block parameters for GPC structures [10, 24]. According to the previous studies by Hardjito and Sarker, a modified Popovics model of stress-strain relationship for conventional concrete can predict accurately the compressive behaviour of GPC [8, 24]. This model is expressed mathematically by Eq. (5)

$$f_c = f\left(\varepsilon_c\right) = f_c^{'} \frac{\varepsilon_c}{\varepsilon_c^{'}} \frac{n}{n-1+\left(\frac{\varepsilon_c}{\varepsilon_c^{'}}\right)^{np}} \tag{5}$$

where f_c is concrete compressive stress, ε_c is compressive strain of concrete, f_c' (in MPa) is the concrete cylinder strength, ε_c' is the concrete strain at f_c which is calculated by Eq. (8), the curve fitting factors n and p are presented in Eqs. (6) and (7), and the elastic modulus of GPC is calculated by using the empirical Eq. (9) proposed by Hardjito [24] as follows:

$$n = 0.8 + \frac{f_c^{'}}{12} \tag{6}$$

$$p = 0.67 + \frac{f_c^{'}}{62} \text{ when } \frac{\varepsilon_c}{\varepsilon_c^{'}} > 1 \text{ and } p = 1 \text{ when } \frac{\varepsilon_c}{\varepsilon_c^{'}} \le 1 \quad (7)$$

$$\varepsilon_c^{'} = \frac{f_c^{'}}{E_c} \frac{n}{n-1} \quad (8)$$

$$E_c = 2707\sqrt{f_c^{'}} + 5300 \text{ (MPa)} \quad (9)$$

Similarly, in an effort to establish a stress-strain relationship for GPC Noushini et al. [10] developed a new model through calibrating the curve-fitting parameters of the Popovics stress-strain curve based on the cylinder compressive test results of 13 GPC specimens. The model is presented in Eqs. (10)-(16), where the modulus of elasticity and strain at peak of GPC is calculated by Eqs. (17) and (18).

$$f_c = f\left(\varepsilon_c\right) = f_c^{'} \frac{\varepsilon_c}{\varepsilon_c^{'}} \frac{n}{n-1+\left(\frac{\varepsilon_c}{\varepsilon_c^{'}}\right)^n} \quad (10)$$

$$n = n_1 = \left[1.02 - 1.17(E_{\text{sec}} / E_c)\right]^{-0.45} \text{ if } \varepsilon_c \le \varepsilon_c^{'} \quad (11)$$

$$n = n_2 = n_1 + \left(\varpi + 28\zeta\right) \text{ if } \varepsilon_c > \varepsilon_c^{'} \quad (12)$$

$$\varpi = C\left(12.4 - 0.015 f_c^{'}\right)^{-0.5} \quad (13)$$

$$\zeta = 0.83 \times \exp(-911 / f_c^{'}) \quad (14)$$

$$C = 17 \text{ for heat cured GPC} \quad (15)$$

$$E_{\text{sec}} = f_c^{'} / \varepsilon_c^{'} \quad (16)$$

$$E_C = -11470 + 4712\sqrt{f_c^{'}} \quad (17)$$

$$\varepsilon_c^{'} = \frac{2.23\times10^{-7}\left(E_c\right)^{1.74}}{\left(f_c^{'}\right)^{1.98}} \tag{18}$$

where the curve fitting factor n is represented by two modified parameters n_1 at the ascending branch (Eq. (11)) and n_2 at the descending branch (Eq. (12)), ϖ and ζ are the necessary coefficients to determine n_1 and n_2, C is the curing parameter which is equal to 17 for GPC under heat curing condition, E_c (Eq. (17) is the modulus of elasticity of GPC in MPa and E_{sec} (Eq. (16)) is the secant modulus. The strain ε_c' at peak stress is calculated by Eq. (18).

The method to establish rectangular stress-block parameters based on analytical stress-strain curves was developed in previous studies for Portland concrete [30, 33, 40, 43]. This method is also adopted in the present study to derive the rectangular stress-block parameters for GPC. In addition, this study also proposes a method to obtain the rectangular stress-block parameters directly from experimental stress-strain curves measured in uniaxial compression tests of cylinder samples. These methods will be presented in the next section.

5. DERIVATION OF RECTANGULAR STRESS-BLOCK PARAMETERS

5.1. ESTABLISHING EQUATIONS FOR RECTANGULAR STRESS-BLOCK PARAMETERS

For the compression zone with the width b and depth to neutral axis c in Fig. 2, the resultant compressive force is

$$C = k_1 f_c^{''} bc = k_1\left(k_3 f_c^{'}\right)bc \tag{19}$$

where the parameter k_3 is a ratio of the real maximum stress f_c'' in compression zone of structural elements to concrete strength of cylinder samples f_c', the parameter k_1 is the ratio of the average compressive stress to the maximum stress f_c'' and the parameter k_2 is the ratio of

the distance between the extreme compression fiber and the internal compressive force C to the depth of the neutral axis.

According to Wight and MacGregor [44], the value of k_1 is determined by dividing the stress-block by the area of rectangle (as illustrated in Fig. 3b). The stress-block area and the area of rectangle are presented mathematically in Eqs. (20) and (21) as follows:

$$\text{Stress-block area} = \int_0^c f_c(\varepsilon_c)dy = \frac{c}{\varepsilon_{cu}}\int_0^{\varepsilon_{cu}} f_c(\varepsilon_c)d\varepsilon_c \tag{20}$$

$$\text{Area of rectangle} = f_c^{''}c = k_3 f_c^{'}c \tag{21}$$

where ε_{cu} is the ultimate strain at extreme compression strip (Fig. 3a) and $f_c(\varepsilon_c)$ (Fig. 3c) is the function that represents the compressive stress–strain relationship for concrete. $f_c(\varepsilon_c)$ can be estimated based on the measured stress-strain curves obtained from concrete cylinder tests or the available analytical stress-strain models. However, Wight and MacGregor [44] suggested that the peak stress f_c' in stress-strain models or curves adopted to calculate stress-block parameters should be $f_c'' = k_3 f_c'$ because there are differences of strengths between the cylinder samples and structural members in real scale (the suitable values of k_3 will be discussed below). Therefore, k_3 diminishes in the equation to determine k_1 by combining Eqs. (20) and (21) as follows:

$$k_1 = \frac{\text{Stress-block area}}{\text{Area of rectangle}} = \frac{\int_0^{\varepsilon_{cu}} f_c(\varepsilon_c)d\varepsilon_c}{f_c^{'}\varepsilon_{cu}} \tag{22}$$

Fig. 3. Illustrations for k_1 determination

With a stress-block illustrated in Fig. 4, the parameter k_2 is calculated by

$$k_2 = \frac{c - \bar{y}}{c} \tag{23}$$

where $\bar{y}$ is distance from the neutral axis to centroid of the stress-block and can be expressed as follows:

$$\bar{y} = \frac{\int_0^c y f(y) dy}{\int_0^c f(y) dy} = \frac{c\int_0^{\varepsilon_{cu}} \varepsilon_c f_c(\varepsilon_c) d\varepsilon_c}{\varepsilon_{cu}\int_0^{\varepsilon_{cu}} f_c(\varepsilon_c) d\varepsilon_c} \tag{24}$$

After substituting $\bar{y}$ in Eq. (24) into Eq. (23), the integral formula of k_2 is

$$k_2 = 1 - \frac{\int_0^{\varepsilon_{cu}} \varepsilon_c f_c(\varepsilon_c) d\varepsilon_c}{\varepsilon_{cu}\int_0^{\varepsilon_{cu}} f_c(\varepsilon_c) d\varepsilon_c} \tag{25}$$

Fig. 4. Relationship of k_2 and centroid of stress-block area $\bar{y}$

If the stress-strain relationship $f_c(\varepsilon_c)$ is known, the parameters k_1 and k_2 can be determined from Eqs. (22) and (25). In this study, two analytical models of GPC in Eq. (5) and Eq. (10) are adopted to represent the stress-strain relationship of concrete. In addition, $f_c(\varepsilon_c)$ can be obtained from measured stress-strain curves in cylinder tests, which were reported in the published studies in the literature [8, 10, 13, 34].

The integrals in Eq. (22) and Eq. (25) depend on the value of the ultimate concrete compressive strain ε_{cu}, so the determination of this parameter is significantly important. In ACI 318-11 standard [28], the value of ε_{cu} is recommended as 0.003 while in the modified Hognestad stress-strain curve, it has the value of 0.0038 . Another way to estimate ε_{cu} is based only on the unit moment $\bar{M}$ caused by compressive stress-block [33], which is expressed by Eqs. (26) and (27). Fig. 5 illustrates the function $\bar{M}$ of variable ε_{cu} when using

the Popovics stress-strain curve. By differentiating $\overline{M}$ at the maximum $\overline{M}_{max}$ value, the value of ε_{cu} can be calculated as shown in Eq. (28). This value is used to calculate integrals in Eqs. (22) and (25).

$$M = k_1(k_3 f_c^{'})cb\left(c - k_2 c\right) \tag{26}$$

$$\overline{M} = \frac{M}{\left(k_3 f_c^{'}\right)c^2 b} = k_1\left(1 - k_2\right) = \frac{\int_0^{\varepsilon_{cu}} \varepsilon_c f\left(\varepsilon_c\right) d\varepsilon_c}{\varepsilon_{cu}^2 f_c^{'}} \tag{27}$$

$$\frac{d\overline{M}}{d\varepsilon_{cu}} = \frac{\varepsilon_{cu}^2 f_c\left(\varepsilon_{cu}\right) - 2\int_0^{\varepsilon_{cu}} \varepsilon_c f\left(\varepsilon_c\right) d\varepsilon_c}{\varepsilon_{cu}^3 f_c^{'}} = 0 \tag{28}$$

Fig. 5. The relationship between $\overline{M}$ and ε_{cu}

For the stress-block with the rectangular shape depicted in Fig. 2b, the resultant compressive force caused by rectangular stress-block parameters α and β can be expressed as follows:

$$C = \alpha\beta f_c^{'} bc \tag{29}$$

Since the resultant compressive force in Eq. (29) must be equal to the value resulted from real stress-block in Eq. (19), the equation for α and β can be written as follows:

$$\alpha\beta = k_1 k_3 \tag{30}$$

Moreover, the rectangular stress-block gives the same internal level arm of real stress-block and thus β is expressed as follows:

$$\beta = 2k_2 \tag{31}$$

By combining Eq. (30) and Eq. (31), α can be expressed as:

$$\alpha = \frac{k_1 k_3}{2k_2} \tag{32}$$

To sum up, the rectangular stress-block parameters α and β can be calculated straightforwardly if the parameters k_1, k_2 and k_3 of real stress-block is known. In order to determine the parameters k_1 and k_2, the integration of Eqs. (22) and (25) must be carried out. The analytical procedures to obtain the solution for these integrals will be described in section 4.3. The value of k_3 will be discussed in section 4.2.

5.2. ASSUMPTION OF THE VALUE OF PARAMETER k_3

According to ACI 318-11 standard [28], the pure ultimate axial load of concrete columns can be computed based on the value of k_3 as follows:

$$P_0 = k_3 f_c^{'}(A_g - A_s) + f_y A_s \tag{33}$$

where P_0 is the ultimate pure axial load, A_g is the gross area of column section, A_s is the total area of longitudinal steel reinforcement steel and f_y is the yield strength of steel reinforcement. The parameter k_3 represents the difference between the concrete compressive strength of a structural element and that of a cylinder sample owing to the change in the shape, size and random factors such as curing condition, vibration during casting, and loading rate, etc. In the ACI 318-11 standard [28], k_3 is recommended to be 0.85. Until now, this parameter has been mainly determined from concentrically loaded column tests [45, 46] and the tests on eccentrically loaded C-shaped columns [35]. Based on these recorded data, Ibrahim and MacGregor [36] recommended that the value of 0.85 for k_3 from the ACI standard was conservative compared to the test findings of eccentrically loaded columns. However, except for columns subjected to pure axial load, the ACI code does not recommend using k_3 for concrete structures under both high axial load and bending moment. Therefore,

Wight and MacGregor [44] proposed the use of $k_3 = 0.9$ according to the previous studies by Pfrang et al. [47] when calculating the combined axial and bending strength of a column section.

In terms of GPC, Sarker [24] used the value $k_3 = 0.9$ to analyse the structural performance of column under axial load and bending moment. The correlation between the results of his analysis and experiment data was quite good. In contrast, Albitar et al. [27] indicated that the use of $k_3 = 0.85$ according to the current standards overestimates the axial load of geopolymer concrete columns by 30%. This difference is attributed to the variation of mixtures and the curing condition. In his study, the content of mixture for GPC consisted of fly ash and granulated lead smelter slag (GLSS) and the columns were cured in ambient condition. Meanwhile, Sarker used the fly ash-based geopolymer concrete columns, which were manufactured in a heat curing condition. This indicates that the use of $k_3 = 0.9$ might be suitable for heat cured fly-ash based GPC columns. For GPC containing another material such as slag and cast in ambient condition, this parameter tends to be smaller than that of the conventional concrete.

From Eq. (33) the parameter k_3 can be estimated by the following expression:

$$k_3 = \frac{P_0 - f_y A_s}{f_c^{'}(A_g - A_s)} \tag{34}$$

where the value of P_0 can be obtained for the concentrically loaded columns. Based on experimental data from column tests in the study by Albitar et al. [27], the authors suggested that k_3 should be 0.7 for the ambient cured GPC. Obviously, it is essential that more studies should be conducted to investigate the factors that govern parameter k_3.

To sum up, regarding the heat cured fly-ash based GPC, k_3 is assumed to be 0.9 for determining the parameter α in Eq. (32) while the value k_3=0.7 is employed in the case of fly-ash and slag based GPC which is cured under ambient condition.

5.3. ANALYTICAL SOLUTIONS OF STRESS-BLOCK EQUATIONS

This section presents the procedures to obtain analytical solutions for equations of rectangular stress-block parameters based on the two aforementioned stress-strain models or experimental curves from cylinder tests. Initially, the analytical stress-strain model by Sarker [24] in Eq. (5) is employed in Eq. (22) and Eq. (25), and hence the formulas of parameters k_1 and k_2 become

$$k_1 = \frac{1}{f_c^{'}\varepsilon_{cu}} \int_0^{\varepsilon_{cu}} f_c^{'} \frac{\varepsilon_c}{\varepsilon_c^{'}} \frac{n}{n-1+\left(\varepsilon_c/\varepsilon_c^{'}\right)^{nk}} d\varepsilon_c = \frac{1}{\varepsilon_{cu}} \int_0^{\varepsilon_{cu}} \frac{n\left(\varepsilon_c/\varepsilon_c^{'}\right)}{n-1+\left(\varepsilon_c/\varepsilon_c^{'}\right)^{nk}} d\varepsilon_c \tag{35}$$

$$k_2 = 1 - \frac{\int_0^{\varepsilon_{cu}} f_c^{'} \frac{\varepsilon_c^2}{\varepsilon_c^{'}} \frac{n}{n-1+\left(\varepsilon_c/\varepsilon_c^{'}\right)^{nk}} d\varepsilon_c}{\varepsilon_{cu} \int_0^{\varepsilon_{cu}} f_c^{'} \frac{\varepsilon_c}{\varepsilon_c^{'}} \frac{n}{n-1+\left(\varepsilon_c/\varepsilon_c^{'}\right)^{nk}} d\varepsilon_c} = 1 - \frac{\varepsilon_c^{'} \int_0^{\varepsilon_{cu}} \frac{n\left(\varepsilon_c/\varepsilon_c^{'}\right)^2}{n-1+\left(\varepsilon_c/\varepsilon_c^{'}\right)^{nk}} d\varepsilon_c}{\varepsilon_{cu} \int_0^{\varepsilon_{cu}} \frac{n\left(\varepsilon_c/\varepsilon_c^{'}\right)}{n-1+\left(\varepsilon_c/\varepsilon_c^{'}\right)^{nk}} d\varepsilon_c} \tag{36}$$

To facilitate later calculation, Eq. (35) and Eq. (36) are rewritten as follows:

$$k_1 = \frac{\varepsilon_c^{'} A}{\varepsilon_{cu}} \tag{37}$$

$$k_2 = 1 - \frac{\varepsilon_c^{'} B}{\varepsilon_{cu} \cdot A} \tag{38}$$

where

$$A = \int_0^{\varepsilon_{cu}/\varepsilon_c'} \frac{nX}{n-1+(X)^{nk}} dX \text{ with } X = \frac{\varepsilon_c}{\varepsilon_c'} \tag{39}$$

$$B = \int_0^{\varepsilon_{cu}/\varepsilon_c'} \frac{nX^2}{n-1+(X)^{nk}} dX \text{ with } X = \frac{\varepsilon_c}{\varepsilon_c'} \tag{40}$$

It is noted that integral expressions in Eqs. (39) and (40) are very complex and it is too difficult to be achieved by analytical solutions. Consequently, a Newton-Cotes numerical integration with the trapezoidal rule [48] is adopted to calculate integrals *A* (Eq. (39)) and *B* (Eq. (40)). Fig. 5 illustrates the application of trapezoidal rule to calculate an integration of an arbitrary stress-strain function. The area is divided into *m* equal segments ($\varepsilon_0 = 0, \varepsilon_1, \varepsilon_2, \ldots, \varepsilon_{m-1}, \varepsilon_m = \varepsilon_{cu}$) and hence, the equal width of each segment is

$$\Delta\varepsilon = \frac{\varepsilon_{cu}}{m} \tag{41}$$

then the total integral can be represented as follows:

$$I \approx \Delta\varepsilon \left(f_c(\varepsilon_0) + 2\sum_1^{m-1} f_c(\varepsilon_i) + f_c(\varepsilon_{cu}) \right) \tag{42}$$

By solving Eq. (43), the integrals *A* (Eq. (39)) and *B* (Eq. (40)) will be determined analytically. The error for the application of the trapezoidal rule will become negligible if the number of divided segments is large enough. In this study, the number of segments is chosen as *m* =100 to ensure the error of numerical integration is smaller than 1%.

Fig. 6. Illustration of numerical integration by using trapezoidal rule

Similarly, the same method to derive parameters k_1 and k_2 will be applied for the stress-strain model by Noushini et al. [10] in Eq. (10). However, when the compressive

strength of cylinders $f_c^{'}$ is greater than 66 MPa, the value of curve fitting factor n_1 in Eq. (11) becomes invalid and then the function cannot be solved. As a result, the solution based on the model by Noushini et al. [10] is only obtained for GPC with compressive strength smaller than 66 MPa. This method can be also employed for measured stress-strain curves with some modifications. Since it is almost impossible to determine an analytical function for an arbitrarily measured stress-strain curve, the calculation of parameters k_1 and k_2 is now conducted by Eq. (22) and Eq. (25) instead of using integrals A (Eq. (39)) and B (Eq. (40)). The use of the trapezoidal rule to calculate the integrals $\int_0^{\varepsilon_{cu}} f_c(\varepsilon_c)\,d\varepsilon_c$ of Eq. (22) and the integrals $\int_0^{\varepsilon_{cu}} \varepsilon_c\, f_c(\varepsilon_c)\,d\varepsilon_c$ of Eq. (25) is based on the value of strain points ($\varepsilon_0 = 0, \varepsilon_1, \varepsilon_2, \ldots, \varepsilon_{m-1}, \varepsilon_m = \varepsilon_{cu}$) and stress points ($f_c(\varepsilon_0)$, $f_c(\varepsilon_1)$, $f_c(\varepsilon_2)$,…, $f_c(\varepsilon_{m-1})$, $f_c(\varepsilon_m) = f_c(\varepsilon_{cu})$) which are obtained directly from the experiment data of cylinder tests [8, 10, 13, 34]. Then Eq. (43) is adopted to derive the parameters k_1 and k_2.

The problem when solving the integrals is that the value of ε_{cu} must be known. To determine ε_{cu}, Eq. (28), which also contains the integrals in mathematical expression of parameters k_1 and k_2, must be solved. For that reason, an iterative procedure developed to calculate ε_{cu}, k_1 and k_2 is presented (Fig. 7) as follows:

Step 1: The area of whole stress-strain curve is divided into m segments, with the value of divided strain points ($\varepsilon_0 = 0, \varepsilon_1, \varepsilon_2, \ldots, \varepsilon_{m-1}, \varepsilon_m = \varepsilon_{cu}$) and stress points (($f_c(\varepsilon_0)$, $f_c(\varepsilon_1)$, $f_c(\varepsilon_2)$,…, $f_c(\varepsilon_{m-1})$, $f_c(\varepsilon_m)$)from analytical models or experimental data;

Step 2: Assign $\varepsilon_{cu} = \varepsilon_i$ (initially, i is equal to 0);

Step 3: Calculate k_1 and k_2 based on Eqs. (37)-(40) (if using the analytical stress-strain models) or Eq. (22) and Eq. (25) (if using the measured curves). The derivative $\frac{d\overline{M}}{d\varepsilon_{cu}}$ is obtained from Eq. (28);

Step 4: Check condition $\frac{d\overline{M}}{d\varepsilon_{cu}} < 0$. If this condition is not satisfied, return to step 2 with new value $i=i+1$;

Step 5: Output the results ε_{cu}, k_1 and k_2.

Fig. 7. Flow chart for the analytical procedure to determine ε_{cu}, k_1 and k_2

Once the parameters k_1 and k_2 are determined, the rectangular stress-block parameters α and β are calculated straightforwardly from Eq. (31) and Eq. (32) associated with the assumption of k_3 discussed in section 5.2. The proposed rectangular stress-block parameters are presented in the next section.

6. PROPOSED RECTANGULAR STRESS-BLOCK PARAMETERS

An analytical algorithm based on the procedures presented in the previous section is developed using the Matlab programming [49] to derive the rectangular stress-block parameters α and β. The results of α and β are shown in Fig. 8 through Fig. 10. Fig. 8 shows the variation of α versus the concrete strength in the case of k_3=0.9 for the heat cured fly-ash based GPC while Fig. 9 illustrates the equations of α for ambient-cured fly-ash and slag based GPC with k_3=0.7. From these figures, the proposed parameter α has a tendency to decrease with the increase of concrete strength instead of being a constant as recommended by ACI 318-11 standard [28]. As a result, this may lead to a more conservative estimation when using ACI 318-11 standard. The variation of β and ε_{cu} is plotted in Fig. 10 and Fig. 11,

respectively. It should be noted that the equations of β and ε_{cu} are the same for both the cases of heat cured fly-ash based GPC and ambient cured fly-ash and slag based GPC because they are independence of k_3. As can be seen from Fig. 10, the values of β according to ACI 318-11 standard [28] are smaller than those estimated from the proposed equations when the concrete compressive strength exceeds 45 MPa. It is worth mentioning that if the value of β is too low, the internal level arm will be too high. Therefore, the design procedure in ACI 318-11 standard likely overestimates the bending moment capacity of GPC structures. However, this does not mean ACI always gives unsafe prediction since the strength estimations of a concrete section still depends on the value of ε_{cu}. ACI 318-11 standard [28] recommends the value of $\varepsilon_{cu} = 0.003$ which is almost the lower bound of analytical results derived from the measured curves (Fig. 11). The common values of ε_{cu} calculated from the measured stress-strain curves vary considerably from 0.0025 to 0.0045. The mean value of regression analysis is about 0.0035 with standard deviation of 8.9634e-04. These results demonstrate that the range of ε_{cu} for GPC is relatively similar to that of OPC. Meanwhile, the equation of ε_{cu} formulated from the modified Popovics model by Sarker [24] is relatively close to the value $\varepsilon_{cu} = 0.003$. The stress-strain model proposed by Noushini et al. [10] yields the highest value of ε_{cu}. This is mainly due to the overestimation of strain at peak stress ε_c' in Eq. (18).

In addition, the proposed parameters α and β derived from the modified Popovics model by Sarker [24] are likely to be the average of values from measured curves while the proposed parameters calculated from model of Noushini et al. [10] have a tendency to be the upper bound. Due to the considerable variation of results between two analytical stress-strain models, this study proposes the equations for α and β by using regression analysis for values obtained from measured curves. These equations are expressed in Eqs. (43)-(45). By taking the mean of all values of ε_{cu} in Fig. 11, Eq. (46) is proposed. Eq. (43) is used for the case of

heat cured fly-ash based GPC while the calculation for the ambient cured fly-ash and slag based GPC is based on Eqs. (44)- (46).

$$\alpha = -4.039\times10^{-6}\left(f_c^{'}\right)^2 - 0.001194\, f_c^{'} + 0.8542 \text{ with } k_3=0.9 \quad (43)$$

$$\alpha = -3.142\times10^{-6}\left(f_c^{'}\right)^2 - 0.0009284\, f_c^{'} + 0.6644 \text{ with } k_3=0.7 \quad (44)$$

$$\beta = -0.002537\, f_c^{'} + 0.8675 \quad (45)$$

$$\varepsilon_{cu} = 0.0035 \quad (46)$$

Fig. 8. Stress-block parameter α in the case of k_3=0.9

Fig. 9. Stress-block parameter α in the case of k_3=0.7

Fig. 10. Stress-block parameter β

Fig. 11. Ultimate concrete strain ε_{cu}

7. EXPERIMENTAL VERIFICATION AND DICUSSION

7.1. FLEXURAL CAPACITY OF BEAMS

The moment capacity of 15 heat cured fly-ash based GPC beams reported in the previous studies [16, 17] is calculated with the proposed rectangular stress-block parameters from Eqs. (43), (45) and (46). The results are compared with calculations based on ACI 318-11 standard [28] and the other stress-block parameters of aforementioned studies [31, 32] (summarized in Table 2). The calculated moment capacity M_{cal} are verified against the experimental data (M_{cal}) reported in those studies. Fig. 12 shows the error δ_b between the

M_{cal} and M_{exp}, where $\delta_b = \frac{M_{\text{cal}} - M_{\text{exp}}}{M_{\text{exp}}} \times 100\%$. In general, the calculated moment capacity indicates a conservative estimation. Despite that both the ACI parameters and parameters proposed by Prachasaree et al. [31] and Tempest et al. [32] differ from the proposed rectangular stress-block parameters of this study, there is no significant difference in the findings of these beams. Therefore, it seems that the calculation of ultimate moment capacity is not sensitive to the variation in stress-block model. Similar observation is also drawn in [33]. In order to clarify this phenomenon, the mathematical relationship between the relative change of moment capacity and the relative difference of parameters α and β needs to be derived.

Table 2-Analytical moment capacity and experimental data

Fig. 12. Error between calculated and experimental moment capacity

It is noted that the bending moment of the beams are estimated based on the equilibrium condition as follows (Fig. 2):

$$T = A_s f_s = \alpha\beta f_c^{'} bc \tag{47}$$

$$M = T\left(d - \frac{\beta c}{2}\right) \tag{48}$$

By combining Eqs. (47) and (48), the bending moment capacity can be calculated by Eq. (49). If the balance condition is achieved, the tension force in the section is a constant so that the bending moment is a function of solely α.

$$M = M(\alpha) = T\left(d - \frac{T}{2\alpha f_c^{'} b}\right) \tag{49}$$

The relative change of moment capacity is expressed mathematically as follows:

$$\frac{\Delta M}{M} = \frac{M(\alpha + \Delta\alpha) - M(\alpha)}{M} = \frac{\Delta\alpha}{(\alpha + \Delta\alpha)\left(\frac{2d\alpha f_c' b}{T} - 1\right)} \tag{50}$$

By substituting the tensile force T in Eq. (47) into Eq. (50), the relative change of moment $\frac{\Delta M}{M}$ is reformulated following Eq. (51) as

$$\frac{\Delta M}{M} = \frac{\Delta\alpha}{\alpha + \Delta\alpha}\frac{1}{\frac{2d}{\beta c} - 1} \tag{51}$$

In Eq. (51), the relative change of the bending moment capacity $\frac{\Delta M}{M}$ is proportional to the relative variation $\frac{\Delta\alpha}{\alpha + \Delta\alpha}$ through a reduced magnitude $\frac{1}{\left(\frac{2d}{\beta c} - 1\right)}$. If the balanced failure happens, that means the strain of longitudinal steel is equal to yield strain, the value of $\frac{d}{c}$ is about 2.67 according to the previous study [44] and then $\frac{1}{\left(\frac{2d}{\beta c} - 1\right)}$ is equal to approximately 0.2. In particular, when the proposed parameter α varies up to 20% as observed in Fig. 13, the value of the bending moment capacity only changes about 4%. From the relationship of $\frac{\Delta M}{M}$ and the ratio of $\frac{d}{c}$ plotted in Fig. 13, it is noted that the ultimate bending moment capacity may change considerably if the ratio $\frac{d}{c}$ becomes smaller. It means that the section of beam is over-reinforced and the compression failure happens. Nevertheless, in design procedures the longitudinal reinforcement ratio of beam is kept less than or equal to 0.75 times balanced reinforcement ratio [28]. As a result, the bending moment capacity will be relatively insensitive to the change of stress-block models if the ratio of reinforcement steel is

selected reasonably. Hence it is suggested that the stress-block parameters of ACI 318-11 standard is acceptable to be used for designing the flexural strength of GPC beams. However, the error in estimating the capacity of GPC structures may become significant for columns, which will be discussed in the following section.

Fig. 13. Relationship between $\frac{\Delta M}{M}$ and *d/c* with $\frac{\Delta\alpha}{\alpha+\Delta\alpha}$ = 20%

7.2. STRENGTH OF COLUMNS UNDER AXIAL LOAD AND BENDING

As mentioned in the previous section, the moment capacity will be more sensitive to the variation of stress-block parameters when the compression failure controls. Therefore, it is likely that the capacity calculation of eccentrically loaded columns will be influenced considerably by the selection of stress-block models. The experimental data of 21 GPC columns collected from the previous studies [23, 27] are presented in Table 3. The interaction diagrams of axial load and bending moment for heat-cured GPC columns are shown in Fig. 14. Those diagrams are computed by the proposed rectangular stress-block parameters of this study, together with those suggested by ACI 318-11 [28] and Karthik and Mander [30]. It is worth mentioning that the load-carrying capacity of heat-cured GPC is very different from ambient-cured GPC at the same compressive strength. The distinguished behaviour of the ambient-cured GPC column is shown in Fig. 15. The expression for the error δ_c between calculated column capacity and experimental values is illustrated in Fig. 16. Accordingly, Fig. 17 shows the comparison of errors as calculated by the proposed rectangular stress-block parameters and the other models for OPC as suggested by ACI 318-11 [28] and Karthik and Mander [30]. In the case of heat cured fly ash based GPC columns, those parameters provided the relatively similar interaction diagrams and the errors δ_c among three models were not significantly distinguishable. The results indicated that the assumption of k_3=0.9 is reasonable and the stress-block distribution of heat cured fly-ash based GPC columns is not much different from conventional concrete columns.

Table 3-The experimental data for GPC columns

With regard to the ambient cured fly-ash and slag based GPC columns, however, all the parameters for conventional concrete suggested by ACI 318-11 [28] and Karthik and Mander [30] overestimate the capacity of column significantly. Particularly, the calculations based on ACI parameters and the model of Karthik and Mander [30] are higher than test results, up to 30% (specimen SLC as shown in Fig. 17f). The proposed parameters with the assumption of k_3=0.9 also gave an unsafe prediction because it does not consider the early spalling of brittle concrete cover in ambient cured GPC columns. In contrast, the proposed parameters with the assumption of k_3=0.7 provided a better estimation with the highest error δ_c=15%. These evidences demonstrate that the value of k_3=0.85 recommended by ACI 318-11 standard [28] or k_3=0.9 from the previous studies of Portland concrete is not accurate to predict the strength of ambient cured fly-ash and slag based GPC columns in real scale at which k_3 of 0.7 should be adopted. Such a loss of strength can be attributed to the cover spalling which was observed in experiment of Albitar et al. [27]. This phenomenon is likely caused by drying shrinkage of the cover concrete [50] which is greatly influenced by curing condition. Moreover, several previous studies indicated that the performance of GPC using the slag mortar was very brittle since it performed a very high drying shrinkage, up to six times compared to OPC [13, 51]. Therefore, the ambient cured fly-ash and slag based GPC structures are likely to perform more poorly than those made from heat cured fly-ash based GPC. The premature spalling of concrete cover in ambient-cured GPC columns is thus attributed to the reduction in the axial loading capacity. The spalling of concrete cover was observed in 11 different ambient-cured GPC columns with various eccentricities as presented in the previous study by Albitar et al. [27]. Due to a considerable distinction between those two cases, this study suggests that only the parameter α with the assumption of k_3=0.7 in Eq. (44) is applied for designing GPC structures to get conservative predictions. Despite that, it is

obviously necessary to conduct more experiments of GPC columns with the same consistent test methods of OPC columns to acquire a reliable correlation between cylinder strength and the real compressive strength in GPC column.

Fig. 14. Interaction diagrams of heat cured fly-ash based GPC columns

Fig. 15. Interaction diagrams of ambient cured fly-ash and slag based GPC columns

Fig. 16. Error δ_c between calculated capacity of column and experimental value

Fig. 17. Comparison of δ_c calculated from proposed rectangular stress-block parameters and other parameters

8. CONCLUSION

An analytical procedure to determine rectangular stress-block parameters and ultimate strain ε_{cu} is proposed. Based on the proposed method, a set of rectangular stress-block parameters for GPC with the range of compressive strength up to 66 MPa is established. The load-carrying capacities of GPC beams and columns are calculated by using the proposed parameters together with available stress-block models for OPC. The results were then compared with test data available in literature. Based the discussion and findings from this study, the following conclusions can be drawn:

1. The moment capacity of beams is not sensitive to the variation of rectangular stress-block parameters. With the balanced reinforcement ratio as recommended in current codes, the moment capacity of beams insignificantly change when stress-block

parameters vary up to 20%. Hence, in designing the flexural capacity of GPC beams, the use of current codes for OPC is still acceptable.

2. The column capacity is sensitive to the variation of the rectangular stress-block parameters which are mainly influenced by k_3. For heat cured fly-ash based GPC columns, the assumption k_3=0.9 is still acceptable. The calculation results indicated that the stress-block distribution of heat cured fly ash based GPC is fairly similar to OPC.
3. In the case of ambient cured fly-ash and slag based GPC columns, the value of k_3 should reduce to 0.7 primarily due to significant strength loss in real scale structure compared to cylinder strength. The load-carrying capacity calculated based on stress-block parameters for OPC is not conservative compared to the test data. In some cases, it overestimates the capacity of columns up to 23%.
4. Based on the comparison of the calculated capacity of columns and experimental data, the proposed rectangular stress-block parameters in this study yield better estimations of the column capacities.

In general, the rectangular stress-block parameters for OPC can be used for GPC beams because the bending capacity is not sensitive to these parameters. However, those for OPC columns cannot be utilized for ambient-cured GPC columns, which are more brittle and exhibited a greater strength loss in real scale column than OPC. Therefore, in order to acquire a better reliable correlation between the compressive strength of real scale column and cylinder strength, it is suggested that more GPC column tests need to be conducted.

9. ACKNOWLEDGEMENTS

The support from Australian Research Council under Grant No DP160104557 is greatly appreciated.

10. NOTATION

A_c = area of core concrete

A_g = gross area of concrete section

A_s = area of longitudinal reinforced steel

α, β = rectangular stress-block parameters

b = breadth of rectangular section for beam and square section for column

c = neutral axis depth

C = internal compressive force

d = effective depth of concrete section

E_c = elastic modulus of concrete

ε_c = compressive strain of concrete in stress-strain model

ε_c' = concrete compressive strain at peak stress

ε_{cu} = ultimate strain at extreme compression fiber

ε_y = yield strain of longitudinal steel

e = the eccentricity of the axial load

f_c' = concrete cylinder compressive strength

f_c = concrete compressive stress in stress-strain model

f_s = tensile stress in longitudinal steel

f_y = yield stress of longitudinal steel

k_1 = ratio that represent the difference between area of real and rectangular stress distribution

k_2 = ratio of the distance between the extreme compression fiber and the internal compressive force C to the depth of the neutral axis c

k_3 = ratio that represent the difference between in-place and cylinder strengths

k_4 = ratio that consider strength loss owing to the cover spalling

ρ_s = steel reinforcement ratio

T_s = internal tensile stress

11. REFERENCES

[1] Benhelal E, Zahedi G, Shamsaei E, Bahadori A. Global strategies and potentials to curb CO2 emissions in cement industry. J Cleaner Prod. 2013;51:142-61.
[2] Khan MZN, Shaikh FUA, Hao Y, Hao H. Synthesis of high strength ambient cured geopolymer composite by using low calcium fly ash. Constr Build Mater. 2016;125:809-20.
[3] Ding Y, Dai J-G, Shi C-J. Mechanical properties of alkali-activated concrete: A state-of-the-art review. Constr Build Mater. 2016;127:68-79.
[4] Wallah SE, Rangan BV. Low-calcium fly ash-based geopolymer concrete: long-term properties, research report GC 2. Perth (Australia): Faculty of Engineering Curtin University of Technology; 2006.
[5] Nath P, Sarker PK. Flexural strength and elastic modulus of ambient-cured blended low-calcium fly ash geopolymer concrete. Constr Build Mater. 2017;130:22-31.
[6] Fernandez-Jimenez AM, Palomo A, Lopez-Hombrados C. Engineering properties of alkali-activated fly ash concrete. ACI Mater J. 2006;103:106-12.
[7] Al-Azzawi M, Yu T, Hadi MNS. Factors Affecting the Bond Strength Between the Fly Ash-based Geopolymer Concrete and Steel Reinforcement. Structures. 2018;14:262-72.

[8] Hardjito D. Studies of fly ash-based geopolymer concrete, PhD Thesis [Thesis (Ph D)]. Perth, Australia: Curtin University of Technology; 2005.
[9] Sofi M, van Deventer JSJ, Mendis PA, Lukey GC. Engineering properties of inorganic polymer concretes (IPCs). Cem Concr Res. 2007;37:251-7.
[10] Noushini A, Aslani F, Castel A, Gilbert RI, Uy B, Foster S. Compressive stress-strain model for low-calcium fly ash-based geopolymer and heat-cured Portland cement concrete. Cem Concr Compos. 2016;73:136-46.
[11] Pan Z, Sanjayan JG, Rangan BV. Fracture properties of geopolymer paste and concrete. Magazine of Concrete Research. 2011;63:763-71.
[12] Sarker PK, Haque R, Ramgolam KV. Fracture behaviour of heat cured fly ash based geopolymer concrete. Materials & Design. 2013;44:580-6.
[13] Thomas RJ, Peethamparan S. Alkali-activated concrete: Engineering properties and stress–strain behavior. Constr Build Mater. 2015;93:49-56.
[14] Ganesan N, Abraham R, Deepa Raj S, Sasi D. Stress–strain behaviour of confined Geopolymer concrete. Constr Build Mater. 2014;73:326-31.
[15] Haider GM, Sanjayan JG, Ranjith PG. Complete triaxial stress–strain curves for geopolymer. Constr Build Mater. 2014;69:196-202.
[16] Sumajouw MDJ, Rangan BV. Low-Calcium Fly Ash-Based Geopolymer Concrete: Reinforced Beams and Columns, Research Report GC. Perth(Australia): Curtin University of Technology; 2006.
[17] Dattatreya J K RN, Sabitha D, Ambily P S, Nataraja MC. Flexural behaviour of reinforced Geopolymer concrete beams. Int J Civ Struct Eng. 2011;2:138–59.
[18] Yost JR, Radlinska A, Ernst S, Salera M, Martignetti NJ. Structural behavior of alkali activated fly ash concrete. Part 2: structural testing and experimental findings. Mater Struct. 2012;46:449-62.
[19] Ng TS, Amin A, Foster SJ. The behaviour of steel-fibre-reinforced geopolymer concrete beams in shear. Magazine of Concrete Research. 2013;65:308-18.
[20] Maranan GB, Manalo AC, Benmokrane B, Karunasena W, Mendis P. Evaluation of the flexural strength and serviceability of geopolymer concrete beams reinforced with glass-fibre-reinforced polymer (GFRP) bars. Eng Struct. 2015;101:529-41.
[21] Un CH, Sanjayan JG, San Nicolas R, van Deventer JSJ. Predictions of long-term deflection of geopolymer concrete beams. Constr Build Mater. 2015;94:10-9.
[22] Nguyen KT, Ahn N, Le TA, Lee K. Theoretical and experimental study on mechanical properties and flexural strength of fly ash-geopolymer concrete. Constr Build Mater. 2016;106:65-77.
[23] Sumajouw DMJ, Hardjito D, Wallah SE, Rangan BV. Fly ash-based geopolymer concrete: study of slender reinforced columns. J Mater Sci. 2006;42:3124-30.
[24] Sarker PK. Analysis of geopolymer concrete columns. Mater Struct. 2008;42:715-24.
[25] Elchalakani M, Karrech A, Dong M, Mohamed Ali MS, Yang B. Experiments and Finite Element Analysis of GFRP Reinforced Geopolymer Concrete Rectangular Columns Subjected to Concentric and Eccentric Axial Loading. Structures. 2018;14:273-89.
[26] Farhan NA, Sheikh MN, Hadi MNS. Experimental Investigation on the Effect of Corrosion on the Bond Between Reinforcing Steel Bars and Fibre Reinforced Geopolymer Concrete. Structures. 2018;14:251-61.
[27] Albitar M, Mohamed Ali MS, Visintin P. Experimental study on fly ash and lead smelter slag-based geopolymer concrete columns. Constr Build Mater. 2017;141:104-12.
[28] ACI Committee 318. Building Code Requirements for Structural Concrete (ACI 318-11). 2011.
[29] Hognestad E, Hanson NW, McHenry D. Concrete distribution in ultimate strength design. ACI Journal Proceedings. 1955;52:455-80.
[30] Karthik M, Mander J. Stress-Block Parameters for Unconfined and Confined Concrete Based on a Unified Stress-Strain Model. J Struct Eng. 2011;137:270-3.
[31] Prachasaree W, Limkatanyu S, Hawa A, Samakrattakit A. Development of Equivalent Stress Block Parameters for Fly-Ash-Based Geopolymer Concrete. Arab J Sci Eng. 2014;39:8549-58.

[32] Tempest B, Gergely J, Skipper A. Reinforced geopolymer cement concrete in flexure: A closer look at stress-strain performance and equivalent stress-block parameters. PCI Journal. 2016;61:30-43.
[33] Attard MM, Stewart MG. A two parameter stress block for high-strength concrete. ACI Struct J. 1998;95:305-17.
[34] Yang K-H, Cho A-R, Song J-K. Effect of water–binder ratio on the mechanical properties of calcium hydroxide-based alkali-activated slag concrete. Constr Build Mater. 2012;29:504-11.
[35] Ibrahim HHH, MacGregor JG. Tests of eccentrically loaded high-strength concrete columns. ACI Struct J. 1996;93:585-94.
[36] Ibrahim HHH, MacGregor JG. Modification of the ACI rectangular stress black for high-strength concrete. ACI Struct J. 1997;94:40-8.
[37] Jae-Hoon L, Hyeok-Soo S. Failure and Strength of High-Strength Concrete Columns Subjected to Eccentric Loads. ACI Struct J. 2000;97:75-85.
[38] Ozbakkaloglu T, Saatcioglu M. Rectangular stress block for high-strength concrete. ACI Struct J. 2004;101:475-83.
[39] Bae S, Bayrak O. Early Cover Spalling in High-Strength Concrete Columns. J Struct Eng. 2003;129:314-23.
[40] Sungjin B, Oguzhan B. Stress Block Parameters for High-Strength Concrete Members. ACI Struct J. 2003;100:626-36.
[41] Hwang S-K, Yun H-D. Effects of transverse reinforcement on flexural behaviour of high-strength concrete columns. Eng Struct. 2004;26:1-12.
[42] van Zijl GPAG, Mbewe PBK. Flexural modelling of steel fibre-reinforced concrete beams with and without steel bars. Eng Struct. 2013;53:52-62.
[43] Oztekin E, Pul S, Husem M. Determination of rectangular stress block parameters for high performance concrete. Eng Struct. 2003;25:371-6.
[44] Wight JK, MacGregor JG. Reinforced concrete : mechanics and design. 6th ed. Boston: Pearson; 2012.
[45] Saatcioglu M, Razvi Salim R. High-Strength Concrete Columns with Square Sections under Concentric Compression. J Struct Eng. 1998;124:1438-47.
[46] Cusson D, Paultre P. High-Strength Concrete Columns Confined by Rectangular Ties. J Struct Eng. 1994;120:783-804.
[47] Pfrang EO, Siess CP, Sozen MA. Load-Moment-Curvature Characteristics of Reinforced Concrete Cross Sections. ACI Journal Proceedings. 1964;61:763-78.
[48] Chapra SC, Canale RP. Numerical methods for engineers. 5th ed. Boston: McGraw-Hill Higher Education; 2006.
[49] Matlab. Matlab R2017a [Computer sofware]. Natick, MA, United States: The Mathworks Inc; 2017.
[50] Collins MP, Mitchell D, MacGregor JG. Structural Design Considerations for High-Strength Concrete. Concrete International. 1993;15:27-34.
[51] Duran Atiş C, Bilim C, Çelik Ö, Karahan O. Influence of activator on the strength and drying shrinkage of alkali-activated slag mortar. Constr Build Mater. 2009;23:548-55.

List of Fig.s

List of tables

Table 1-Summary of experimental data of compressive cylinder tests

Specimen designation	Curing		f_c' (MPa)	E_c(Gpa)	Reference
	Temp (^{o}C)	Length (hour)			
Mixture-23	90	24	64	30.6	[8]
Mixture-24	90	24	61	30.8	[8]
Mixture-26	60	24	41	24.7	[8]
GPC-SAC	22	-	41.7	19.3	[10]
GPC-HC-1	60	8	27.4	13.5	[10]
GPC-HC-2	60	12	37.8	16.6	[10]
GPC-HC-3	60	18	45.6	20.3	[10]
GPC-HC-4	60	24	50	22.9	[10]
GPC-HC-5	75	8	44.8	20.4	[10]
GPC-HC-6	75	12	53.9	22.8	[10]
GPC-HC-7	75	18	60	24.4	[10]
GPC-HC-8	75	24	62.3	25.9	[10]
GPC-HC-9	90	8	52.2	23.5	[10]
GPC-HC-10	90	12	58.6	23.9	[10]
GPC-HC-11	90	18	59.8	25.1	[10]
GPC-HC-12	90	24	60.7	25.8	[10]
FC1-22 ^{o}C	22	-	28.9	21.5	[13]
FC1-50 ^{o}C	50	48	47.7	26	[13]
GGBFS5-22 ^{o}C	22	-	45.7	22.4	[13]
GGBFS5-50 ^{o}C	50	48	48.7	22.9	[13]
S-25	22	-	42.2	31.5	[34]
S-30	22	-	28.5	25.3	[34]
C-28	22	-	37.1	29.9	[34]
C-30	22	-	24.2	21.6	[34]

Note: Temp= curing temperature (if temp=22, the specimens were cured in temperature room until the test date), length= the period of time for curing, f_c'= compressive strength at 28 days, E_c=modulus of elasticity.

Table 2-Analytical moment capacity and experimental data

Specimen	Reference	f_c' (MPa)	ρ_s (%)	Bending moment capacity M (MPa)				
				ACI 318-11	Prachasaree et al. [31]	Brett et al. [32]	Proposed	Test
GBI-1	[16]	37	0.64	47.56	49.27	47.41	46.24	56.3
GBI-2	[16]	42	1.18	78.08	79.35	78.89	77.71	87.65
GBI-3	[16]	42	1.84	115.52	117.73	117.56	114.81	116.85
GBI-4	[16]	37	2.69	145.97	156.14	145.67	148.10	162.5
GBII-1	[16]	46	0.64	50.92	52.62	51.64	50.48	58.35
GBII-2	[16]	53	1.18	79.49	80.56	80.80	79.22	90.55
GBII-3	[16]	53	1.84	118.74	120.05	121.48	117.54	119
GBII-4	[16]	46	2.69	156.98	160.34	161.53	155.47	168.7
GBIII-1	[16]	76	0.64	61.46	63.41	54.60	59.63	64.9
GBIII-2	[16]	72	1.18	81.78	83.97	83.09	80.60	92.9
GBIII-3	[16]	72	1.84	122.3	123.22	125.47	120.81	126.8
GBIII-4	[16]	76	2.69	168.39	170.30	175.07	165.60	179.95
FAB-1	[17]	17	1.95	9	9.53	8.72	9.05	8.44
FAB-2	[17]	49	2.92	14.94	15.20	15.39	14.78	19.07
FAB-3	[17]	52	3.53	17.07	17.36	17.67	16.83	20.21

Note: all specimens GBI-1 to GBIII-4 of reference [16] were kept at room temperature for three days and then and cured at 60 ^{o}C for 24 hours, specimens FAB-1 to FAB-3 of reference [17] were cured at room temperature for 28 days.

Table 3-Experimental data for GPC columns

Column	Reference	b (mm)	f_c' (MPa)	e (mm)	Δ_{mid} (mm)	P_u (kN)	M_u (kN.m)
GCI	[23]	175	42	15	5.44	940	19.21
GCI	[23]	175	42	35	8.02	674	29.00
GCI	[23]	175	42	50	10.31	555	33.47
`GCII	[23]	175	43	15	6.24	1237	26.27
GCII	[23]	175	43	35	9.08	852	37.56
GCII	[23]	175	43	50	9.40	666	39.56
GCIII	[23]	175	66	15	4.94	1455	29.01
GCIII	[23]	175	66	35	7.59	1030	43.87
GCIII	[23]	175	66	50	10.70	827	50.20
GCIV	[23]	175	59	15	5.59	1559	32.1
GCIV	[23]	175	59	30	7.97	1057	45.42
GCIV	[23]	175	59	50	9.18	810	47.94
SHC	[27]	150	35	0	0.73	776	0.57
SHC	[27]	150	35	10	3.58	545	7.40
SHC	[27]	150	35	35	6.16	355	14.61
SHC	[27]	150	35	50	8.52	272	15.94
SHC	[27]	150	35	85	10.83	170	16.32
SLC	[27]	150	30	0	0.5	597	0.3
SLC	[27]	150	30	30	9.69	303	12.01
SLC	[27]	150	30	125	20.48	92	13.37
SLC	[27]	150	30	145	19.66	76	12.56

Note: all specimens GCI to GCIV of reference [23] were cured at 60 ^{o}C for 24 hours while specimens SHC and SLC of reference [27] were ambient cured for 56 days prior to testing.

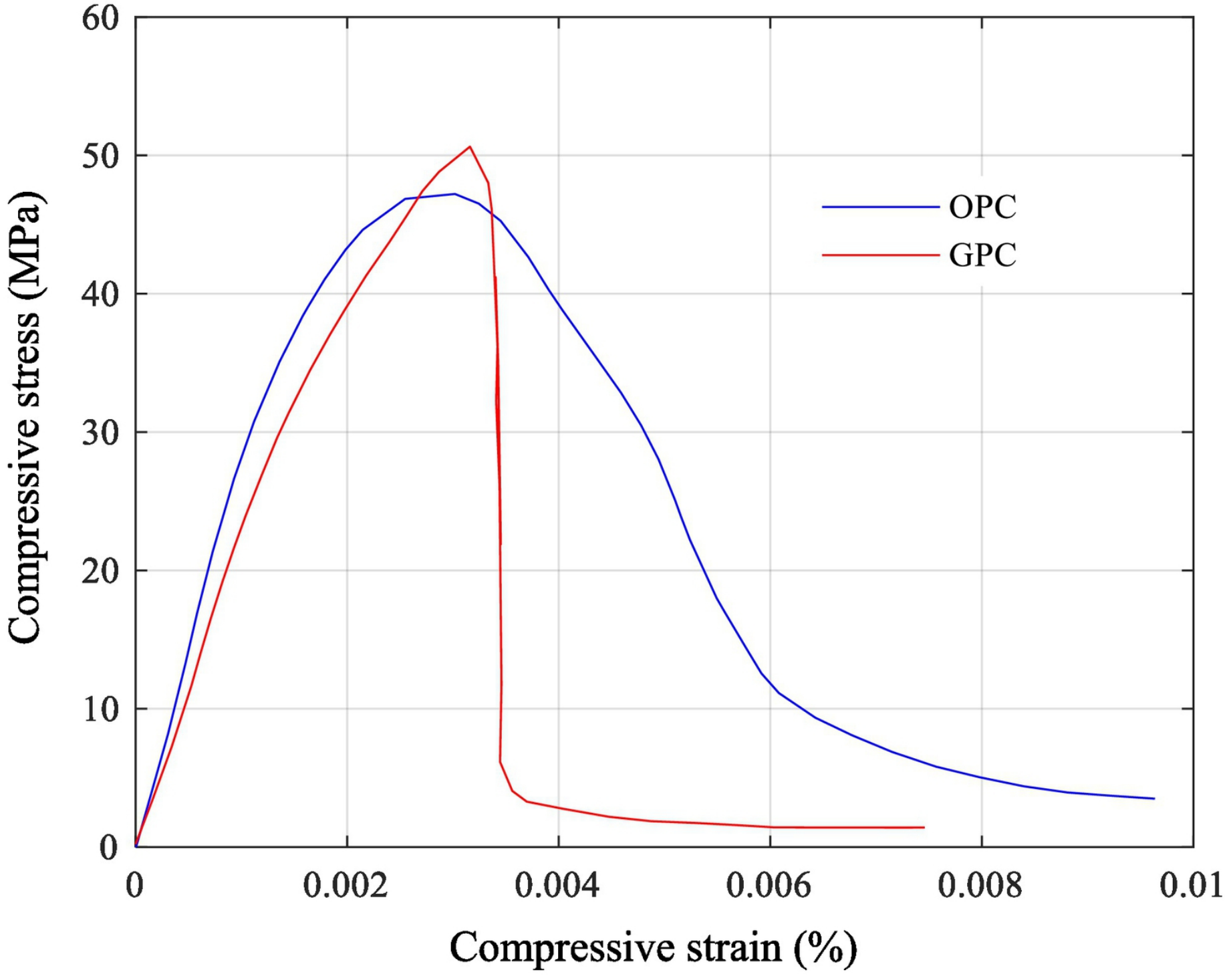
60
50
40
30
20
10
0
0
0.002
0.004
0.006
0.008
0.01
Compressive stress (MPa)
Compressive strain (%)
OPC
GPC

Figure 1

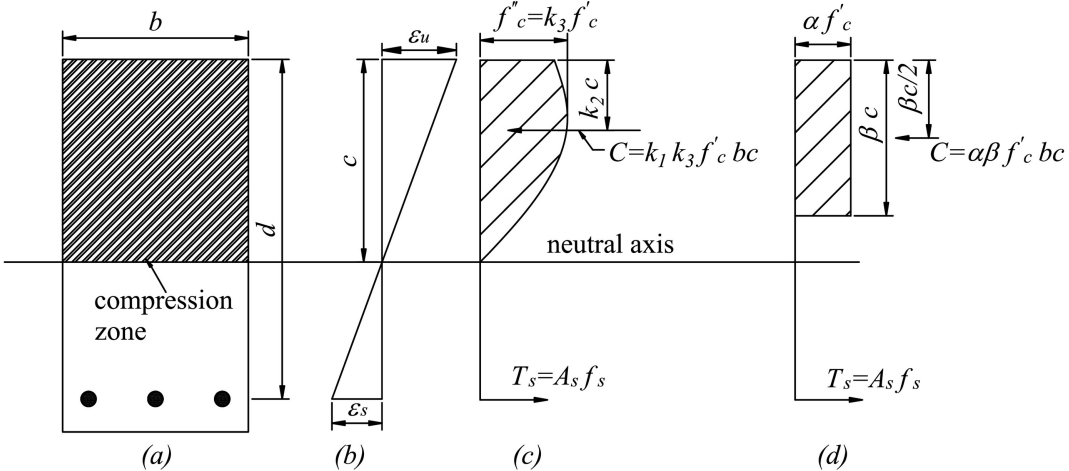
b
d
compression zone
(a)
εu
c
εs
(b)
f″c=k3 f′c
k2 c
C=k1 k3 f′c bc
neutral axis
Ts=As fs
(c)
α f′c
β c
βc/2
C=αβ f′c bc
Ts=As fs
(d)

Figure 2

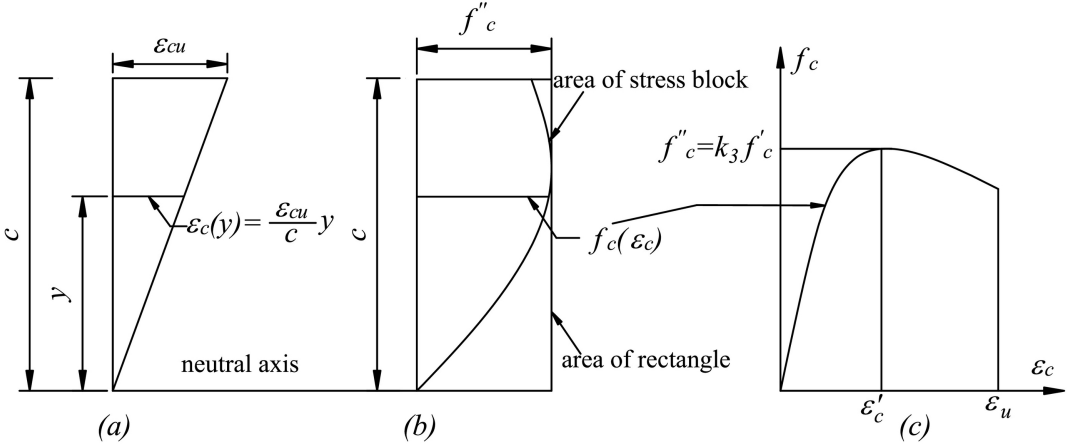
εcu
c
y
εc(y)= εcu/c y
neutral axis
(a)
f''c
area of stress block
c
fc(εc)
area of rectangle
(b)
fc
f''c=k3f'c
εc
ε'c
εu
(c)

Figure 3

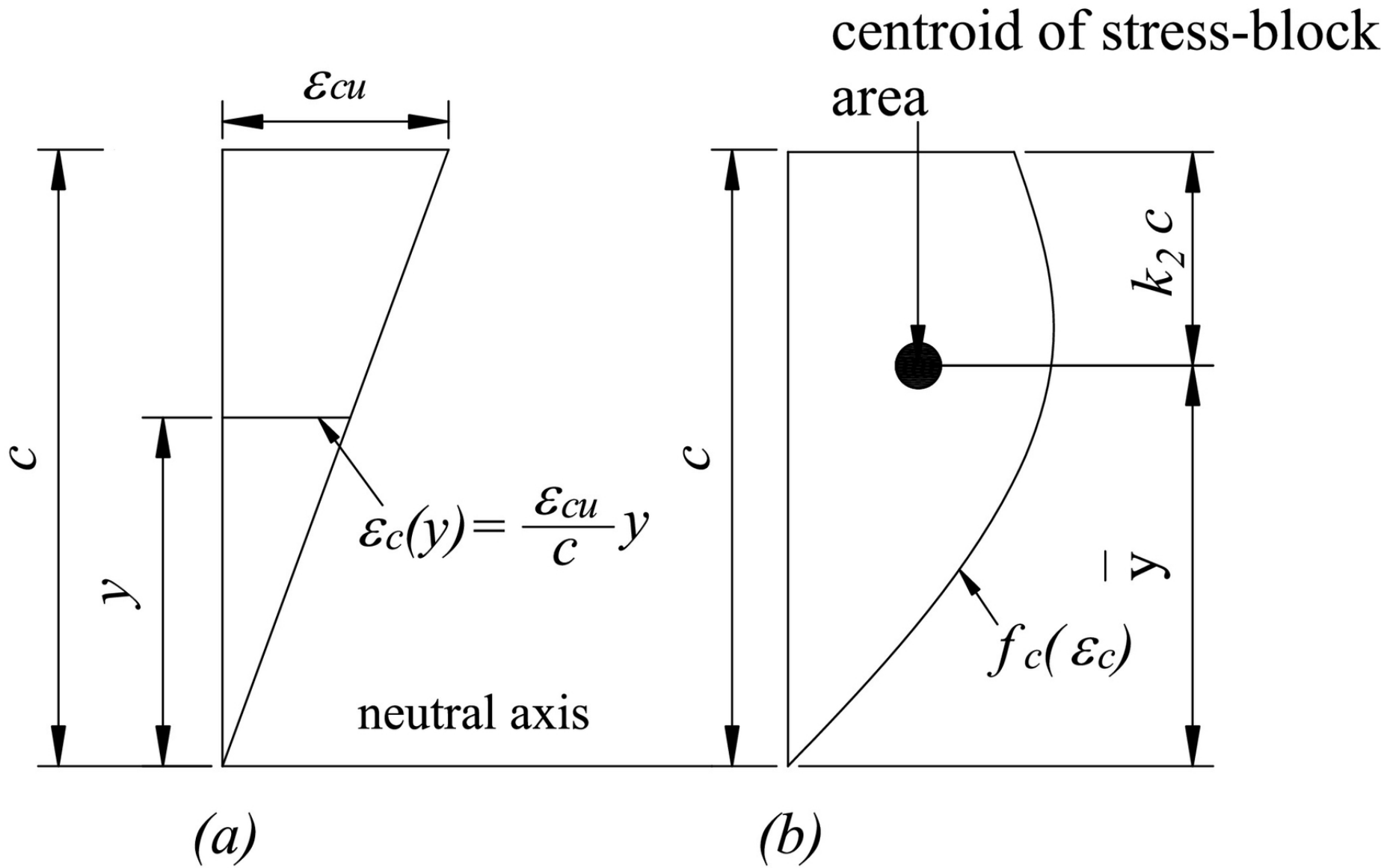
centroid of stress-block area
ε_{cu}
c
y
$\varepsilon_c(y) = \frac{\varepsilon_{cu}}{c} y$
neutral axis
(a)
c
$k_2 c$
y
$f_c(\varepsilon_c)$
(b)

Figure 4

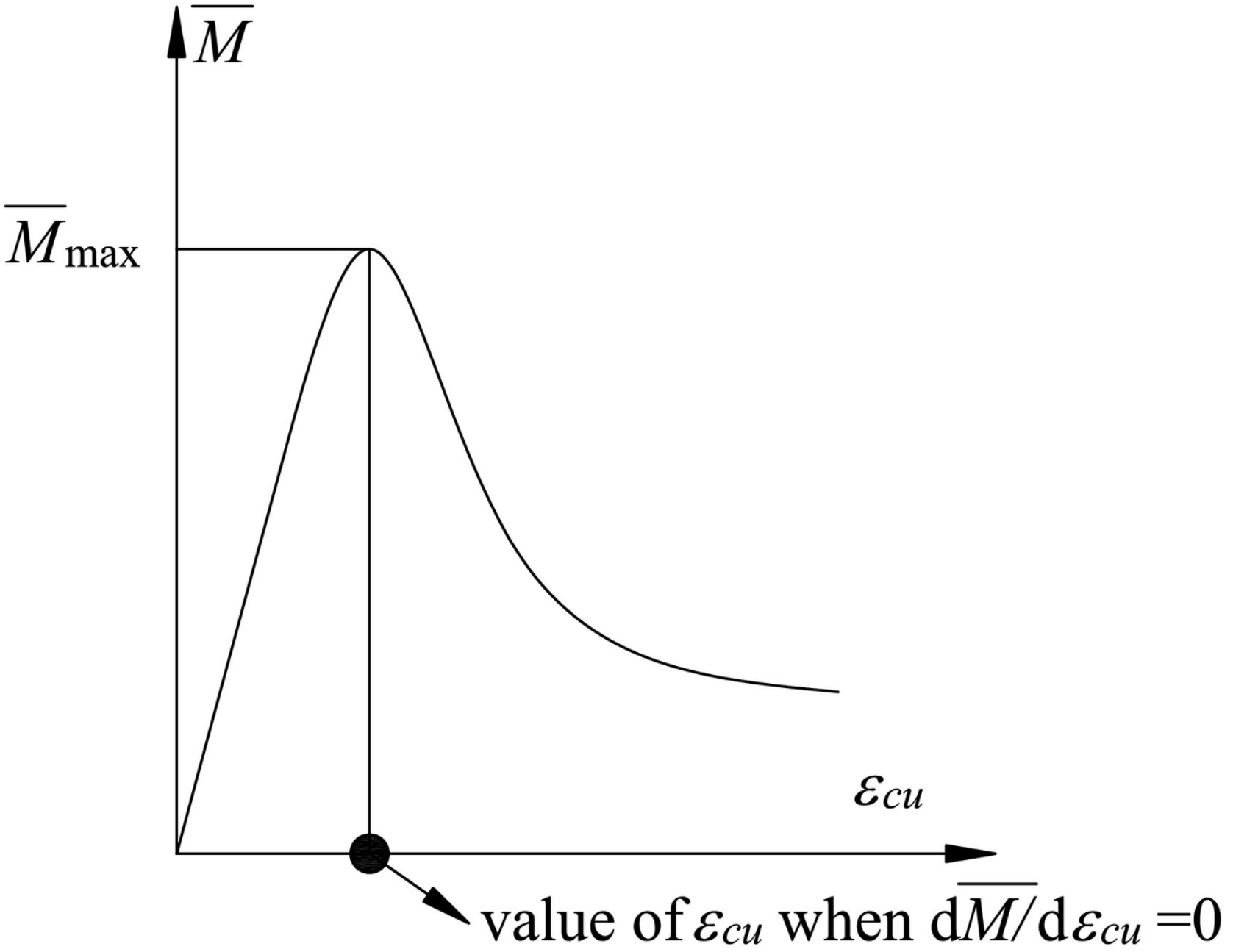
$\overline{M}$
$\overline{M}_{\max}$
ε_{cu}
value of ε_{cu} when $\mathrm{d}\overline{M}/\mathrm{d}\varepsilon_{cu}=0$

Figure 5

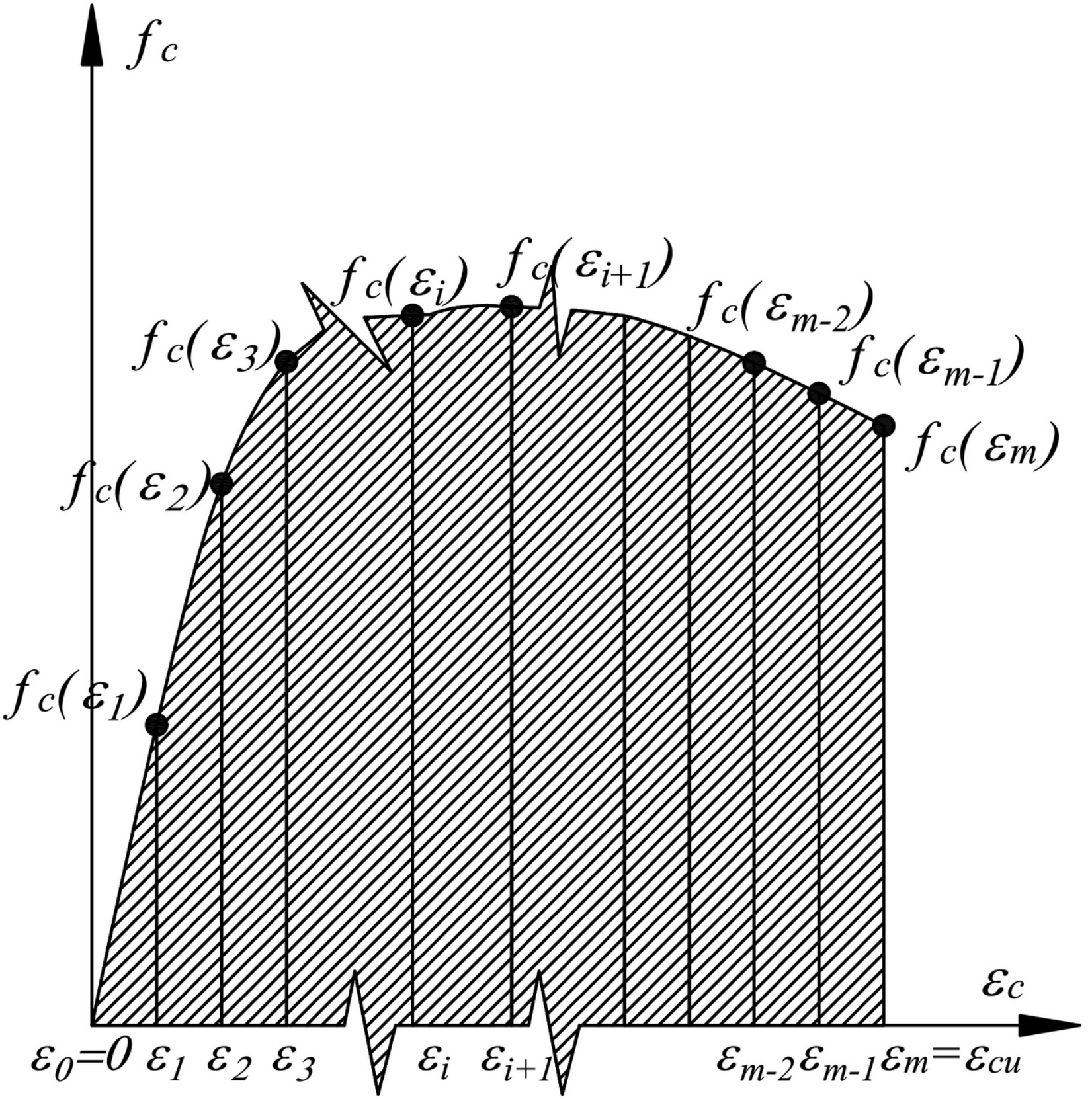
f_c
$f_c(\varepsilon_i)$
$f_c(\varepsilon_{i+1})$
$f_c(\varepsilon_{m-2})$
$f_c(\varepsilon_3)$
$f_c(\varepsilon_{m-1})$
$f_c(\varepsilon_m)$
$f_c(\varepsilon_2)$
$f_c(\varepsilon_1)$
ε_c
$\varepsilon_0=0$ ε_1 ε_2 ε_3
ε_i ε_{i+1}
$\varepsilon_{m-2}\varepsilon_{m-1}\varepsilon_m=\varepsilon_{cu}$

Figure 6

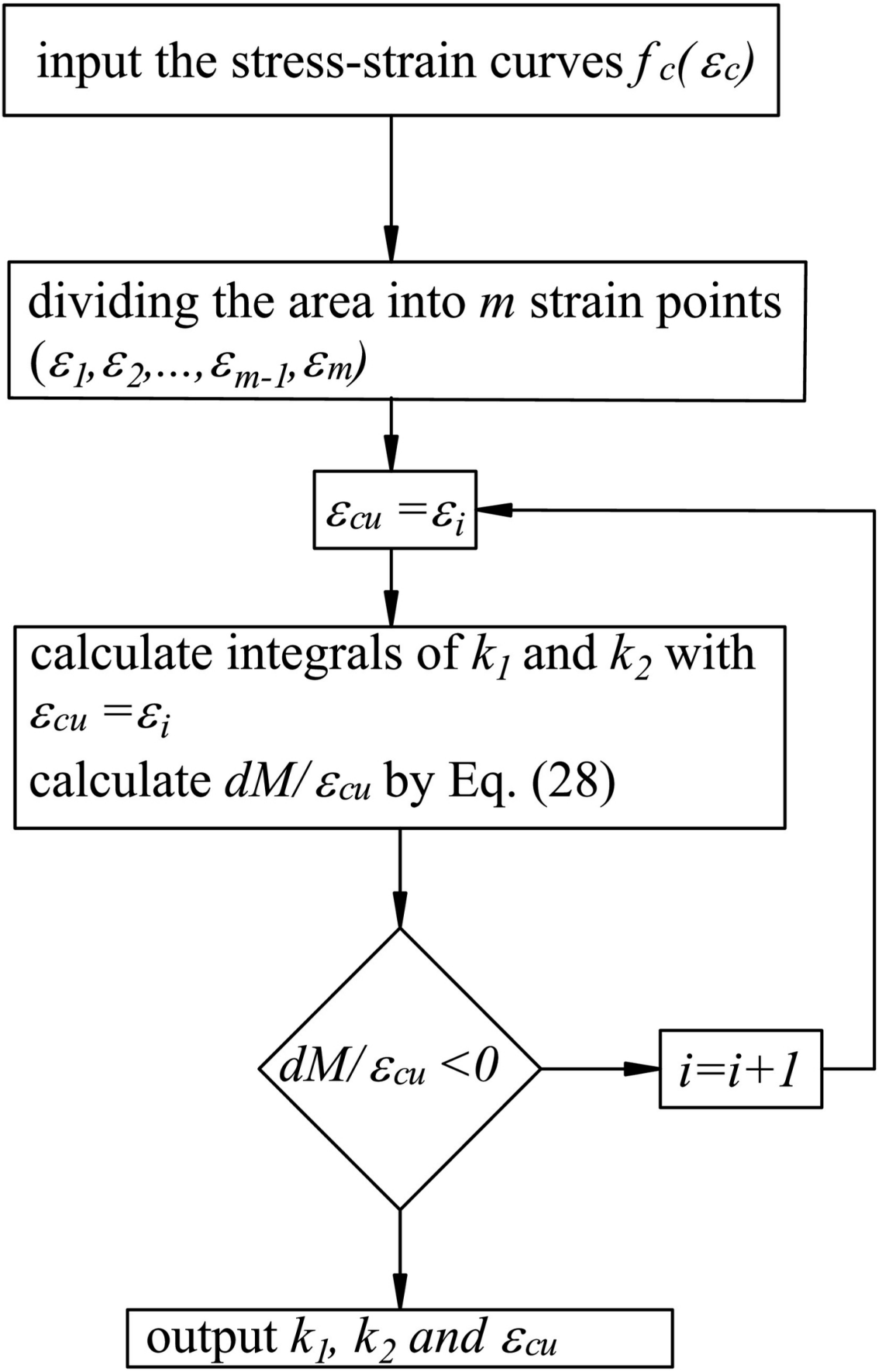
input the stress-strain curves $f_c(\varepsilon_c)$
dividing the area into m strain points $(\varepsilon_1, \varepsilon_2, \ldots, \varepsilon_{m-1}, \varepsilon_m)$
$\varepsilon_{cu} = \varepsilon_i$
calculate integrals of k_1 and k_2 with $\varepsilon_{cu} = \varepsilon_i$
calculate dM/ε_{cu} by Eq. (28)
$dM/\varepsilon_{cu} < 0$
$i=i+1$
output k_1, k_2 and ε_{cu}

Figure 7

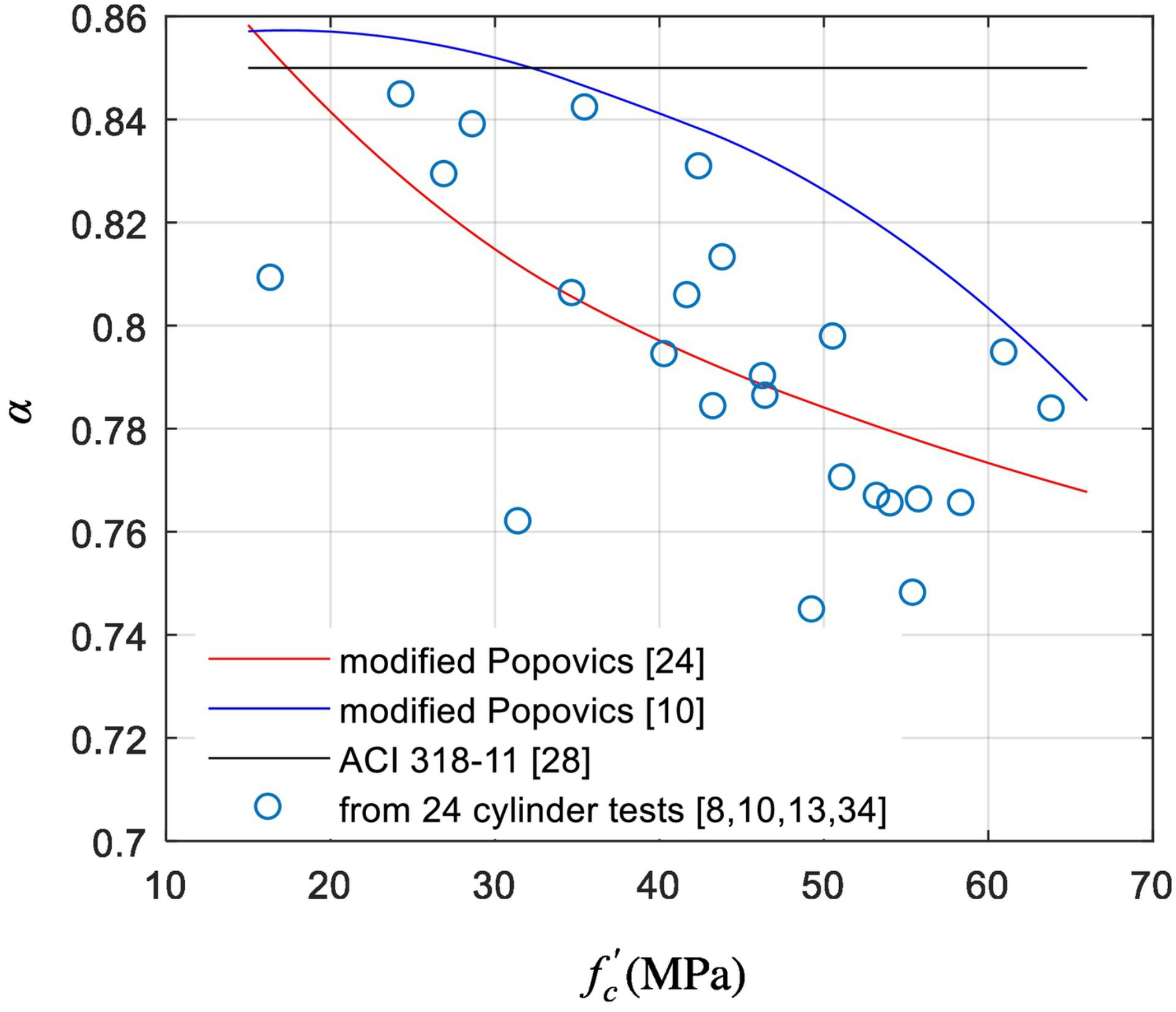
0.86
0.84
0.82
0.8
0.78
0.76
0.74
0.72
0.7
α
10
20
30
40
50
60
70
f_c'(MPa)
modified Popovics [24]
modified Popovics [10]
ACI 318-11 [28]
from 24 cylinder tests [8,10,13,34]

Figure 8

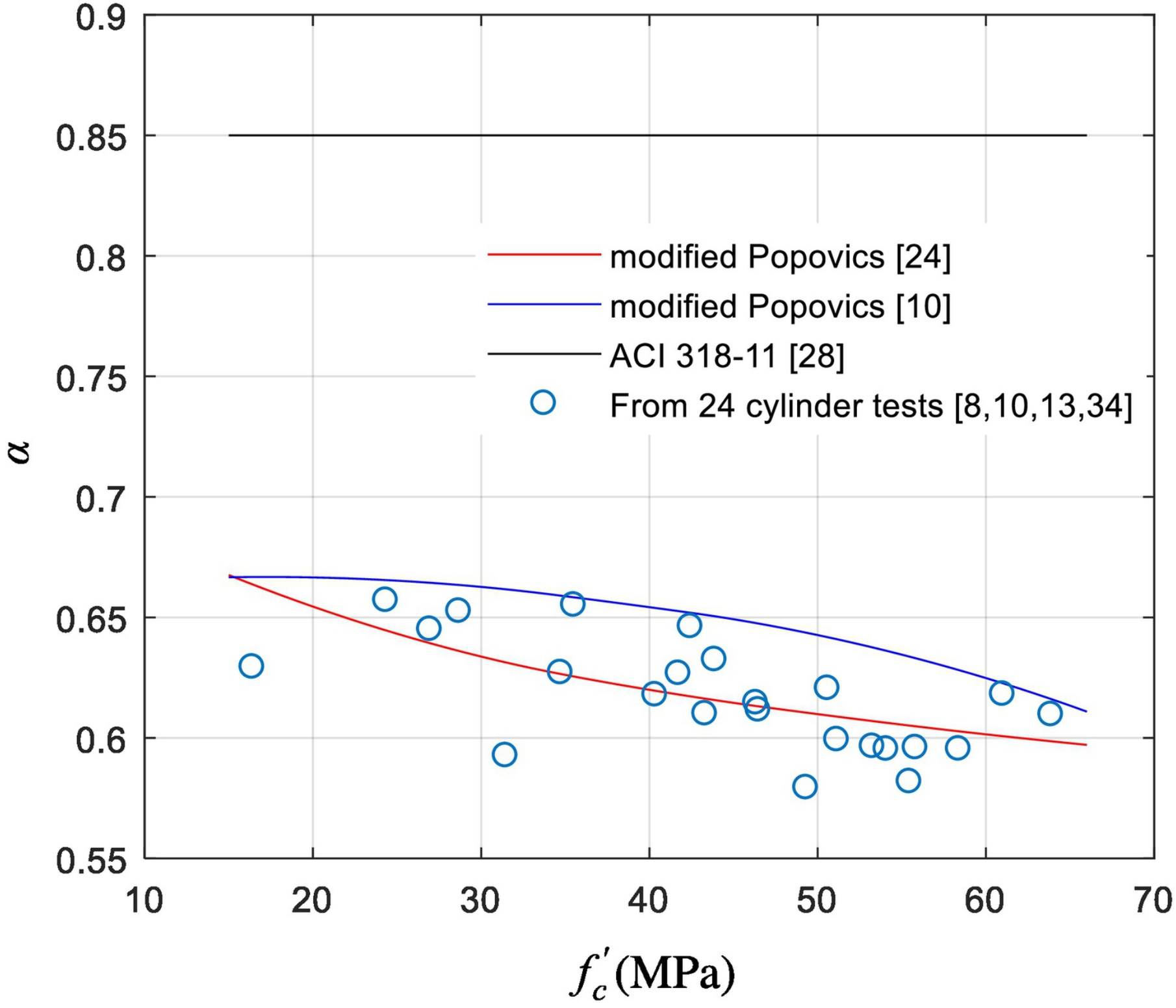
0.9
0.85
0.8
0.75
0.7
0.65
0.6
0.55
α
10
20
30
40
50
60
70
f_c'(MPa)
modified Popovics [24]
modified Popovics [10]
ACI 318-11 [28]
From 24 cylinder tests [8,10,13,34]

Figure 9

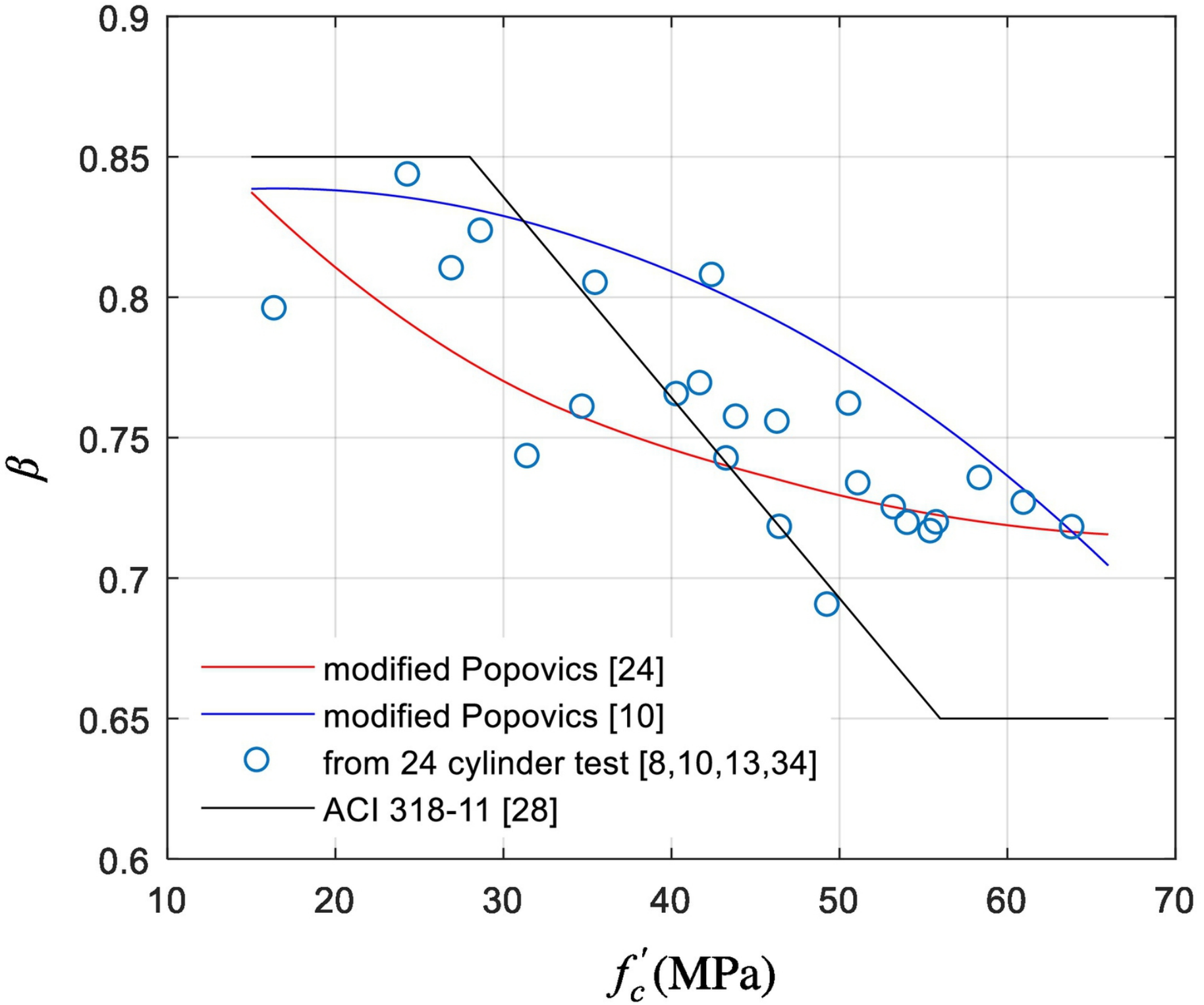
0.9
0.85
0.8
0.75
0.7
0.65
0.6
β
10
20
30
40
50
60
70
f_c'(MPa)
modified Popovics [24]
modified Popovics [10]
from 24 cylinder test [8,10,13,34]
ACI 318-11 [28]

Figure 10

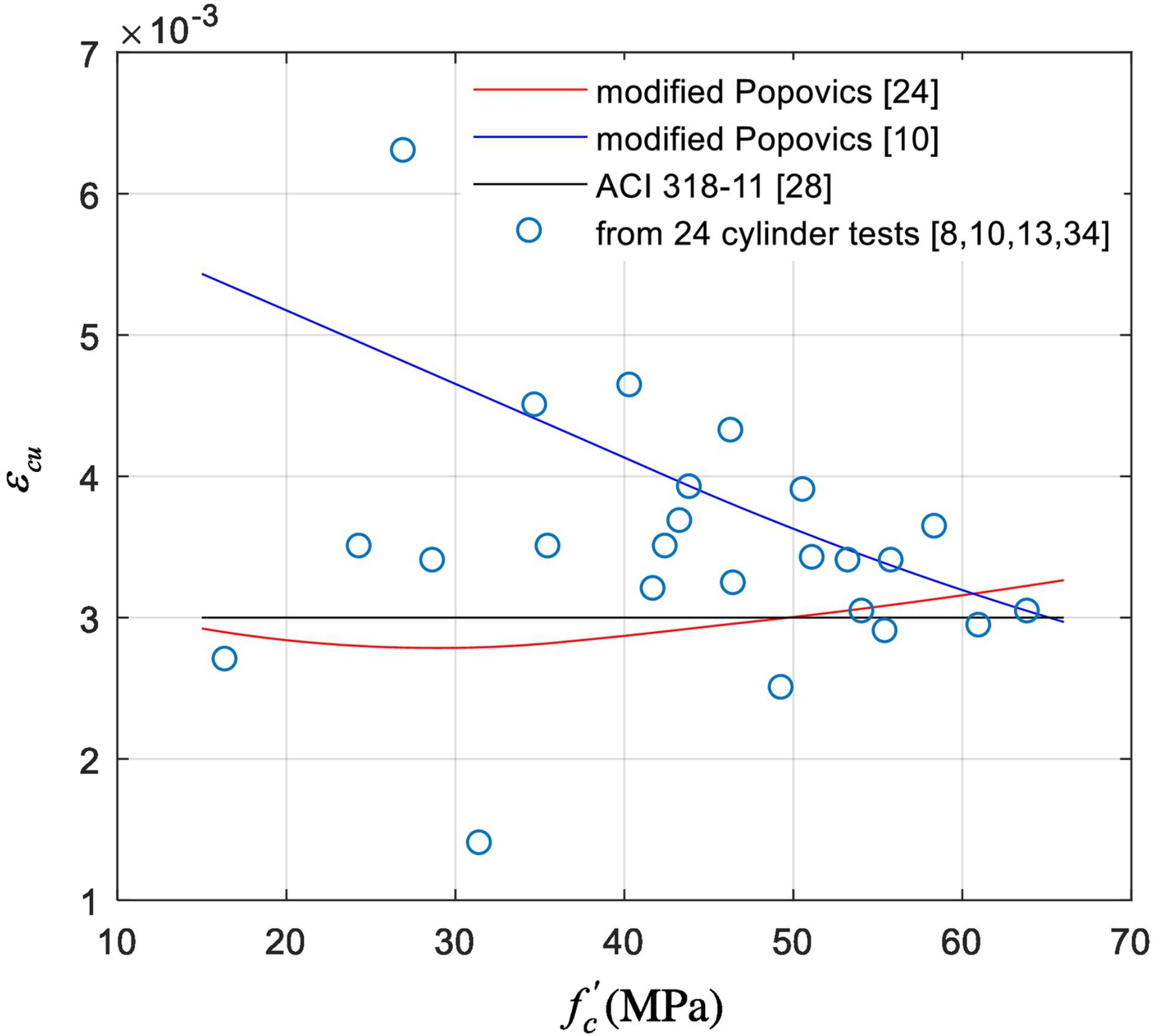
×10-3
7
6
5
4
3
2
1
10
20
30
40
50
60
70
modified Popovics [24]
modified Popovics [10]
ACI 318-11 [28]
from 24 cylinder tests [8,10,13,34]
ε_{cu}
f_c'(MPa)

Figure 11

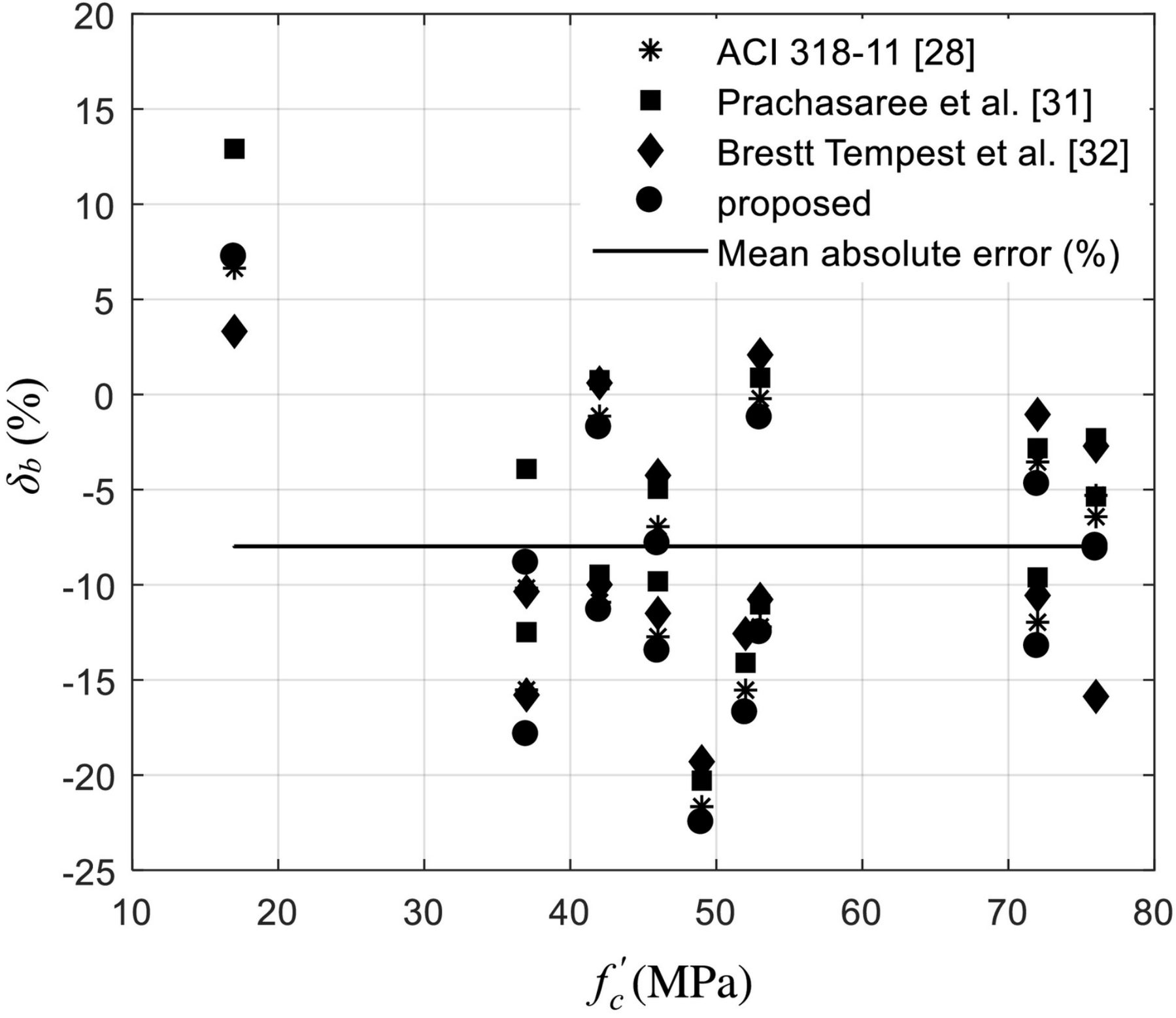
ACI 318-11 [28]
Prachasaree et al. [31]
Brestt Tempest et al. [32]
proposed
Mean absolute error (%)
δ_b (%)
f_c' (MPa)
20
15
10
5
0
-5
-10
-15
-20
-25
10
20
30
40
50
60
70
80

Figure 12

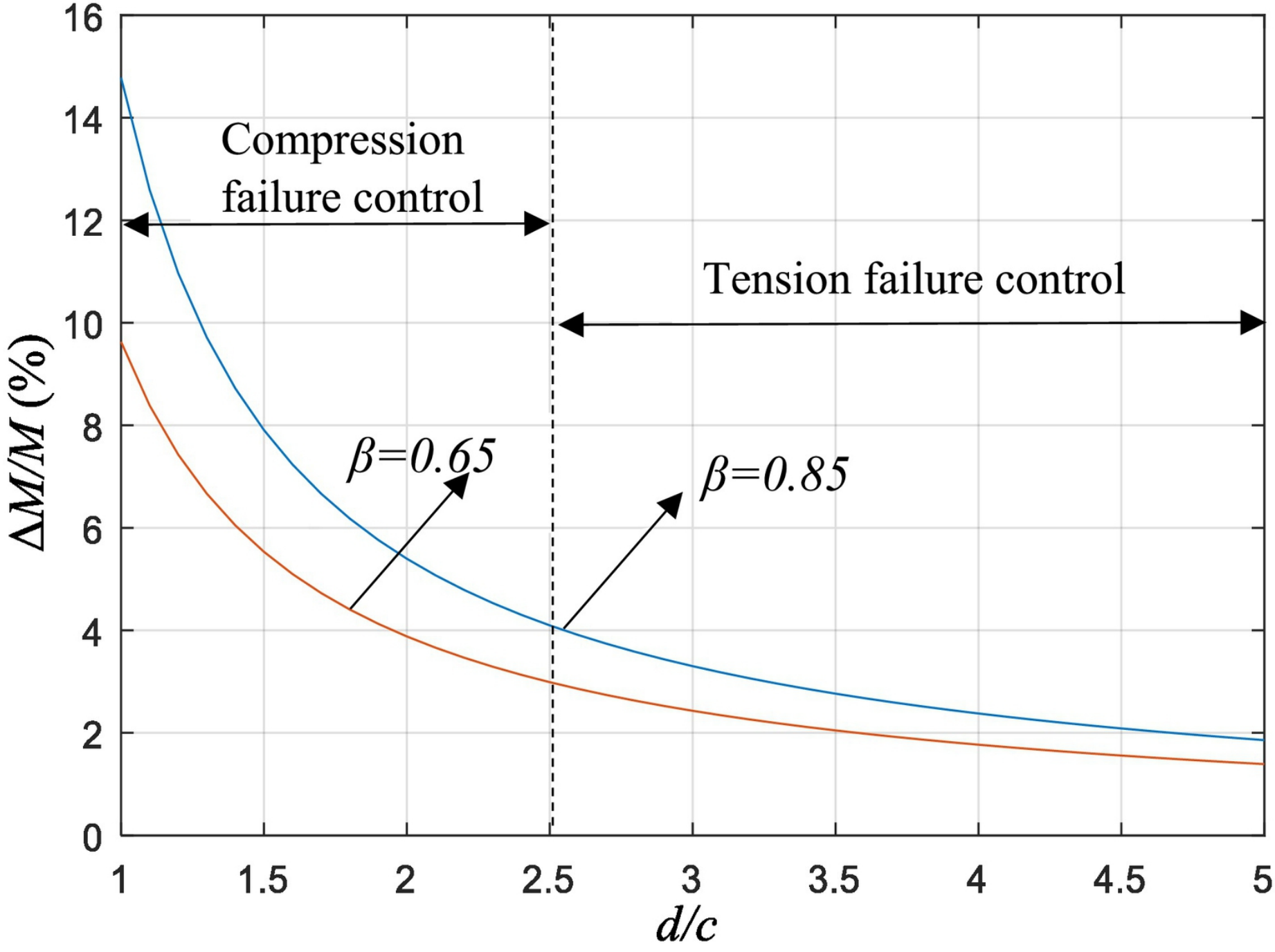
16
14
12
10
8
6
4
2
0
ΔM/M (%)
Compression
failure control
Tension failure control
β=0.65
β=0.85
1
1.5
2
2.5
3
3.5
4
4.5
5
d/c

Figure 13

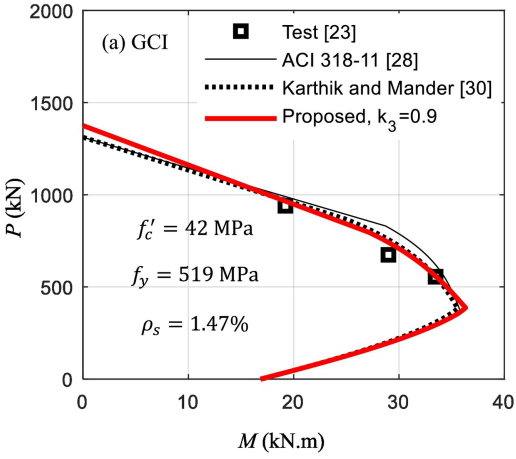
(a) GCI
Test [23]
ACI 318-11 [28]
Karthik and Mander [30]
Proposed, k3=0.9
f'c = 42 MPa
fy = 519 MPa
ρs = 1.47%
P (kN)
M (kN.m)

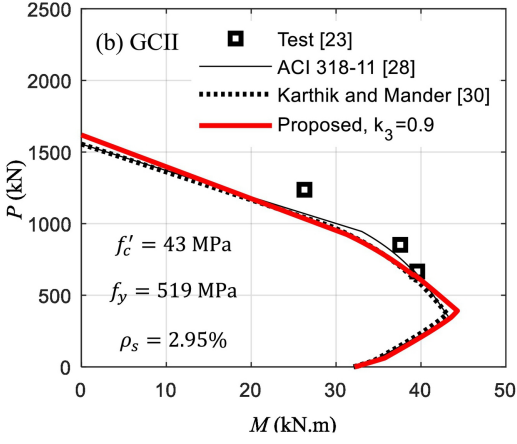
(b) GCII
Test [23]
ACI 318-11 [28]
Karthik and Mander [30]
Proposed, k3=0.9
f'c = 43 MPa
fy = 519 MPa
ρs = 2.95%
P (kN)
M (kN.m)

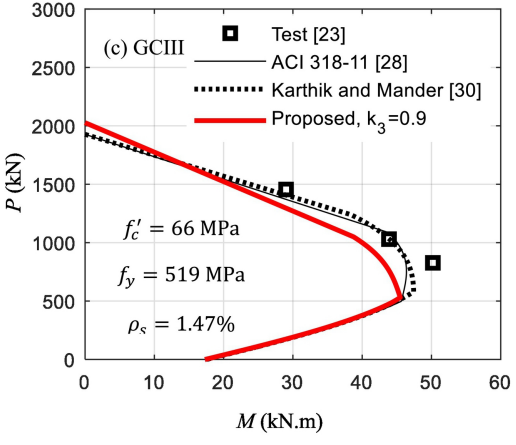
(c) GCIII
Test [23]
ACI 318-11 [28]
Karthik and Mander [30]
Proposed, k3=0.9
f'c = 66 MPa
fy = 519 MPa
ρs = 1.47%
P (kN)
M (kN.m)

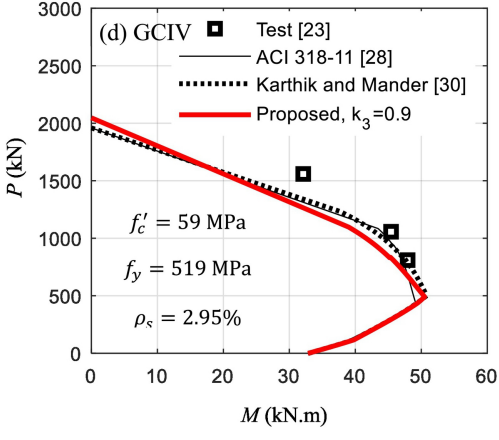
(d) GCIV
Test [23]
ACI 318-11 [28]
Karthik and Mander [30]
Proposed, k3=0.9
f'c = 59 MPa
fy = 519 MPa
ρs = 2.95%
P (kN)
M (kN.m)

Figure 14

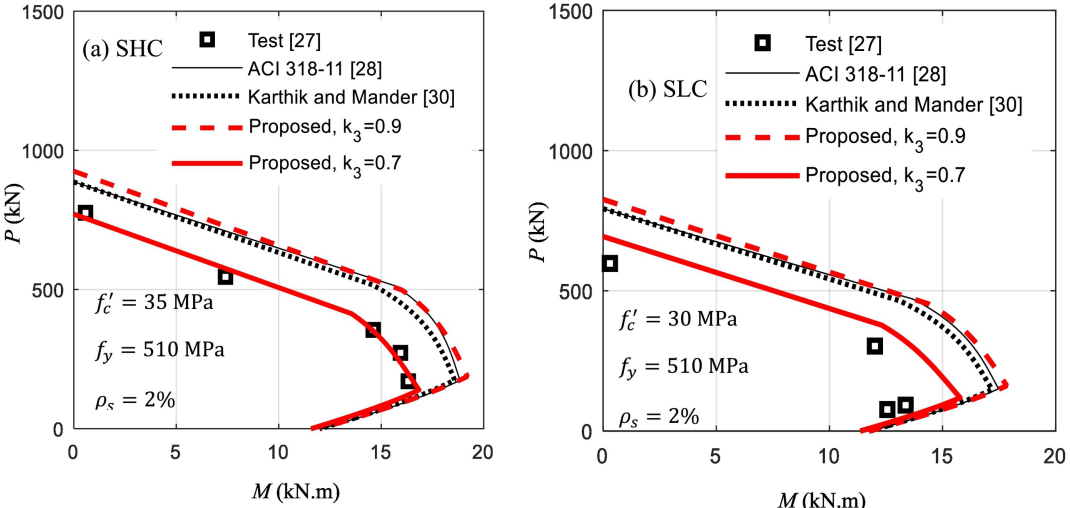
(a) SHC
Test [27]
ACI 318-11 [28]
Karthik and Mander [30]
Proposed, k3=0.9
Proposed, k3=0.7
f'c = 35 MPa
fy = 510 MPa
ρs = 2%
P (kN)
M (kN.m)
(b) SLC
Test [27]
ACI 318-11 [28]
Karthik and Mander [30]
Proposed, k3=0.9
Proposed, k3=0.7
f'c = 30 MPa
fy = 510 MPa
ρs = 2%
P (kN)
M (kN.m)

Figure 15

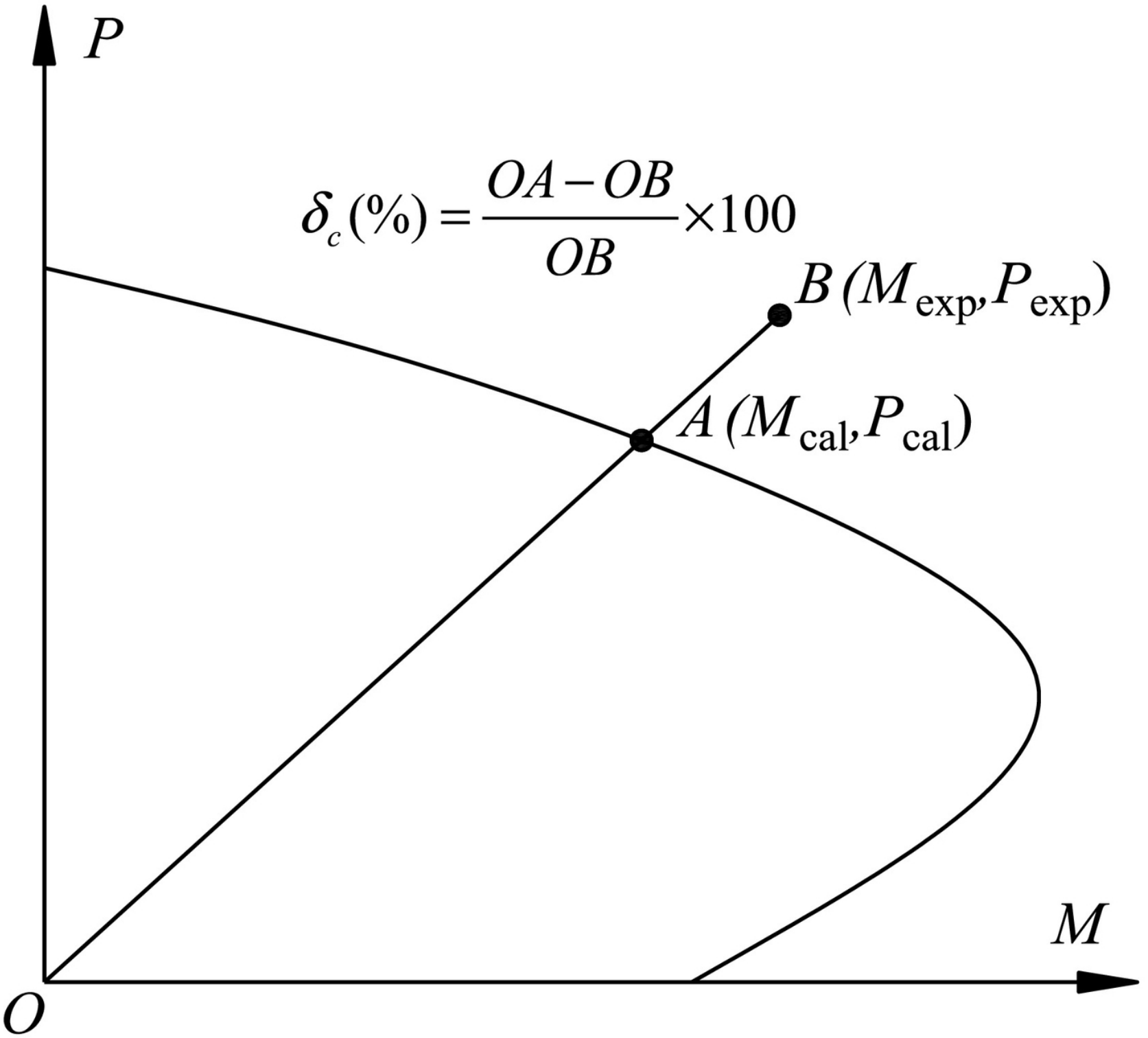
P
$\delta_c(\%) = \frac{OA - OB}{OB} \times 100$
$B(M_{\text{exp}}, P_{\text{exp}})$
$A(M_{\text{cal}}, P_{\text{cal}})$
M
O

Figure 16

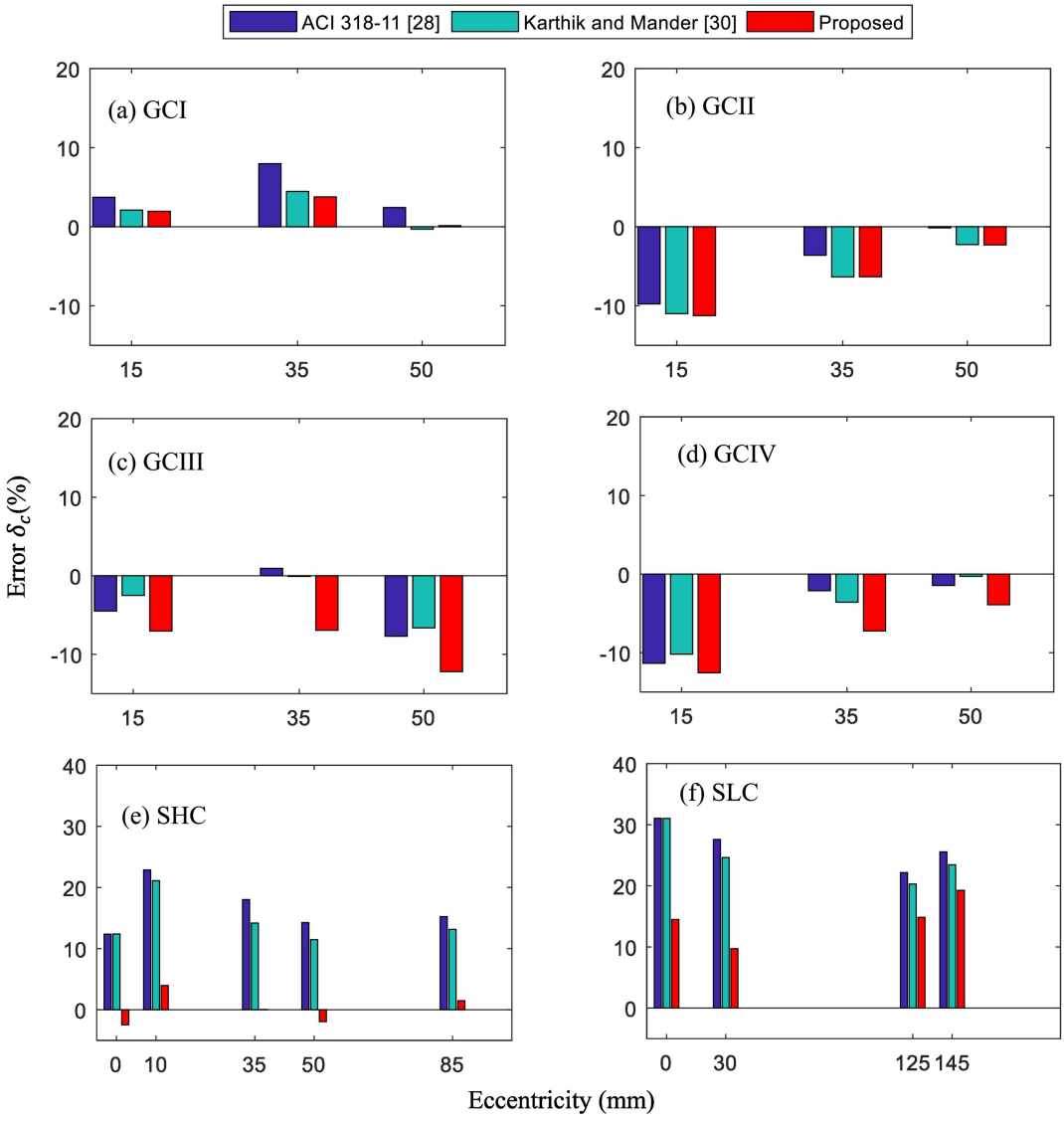
ACI 318-11 [28]
Karthik and Mander [30]
Proposed
(a) GCI
(b) GCII
(c) GCIII
(d) GCIV
(e) SHC
(f) SLC
Error δ_c(%)
Eccentricity (mm)

Figure 17